

HYDRODYNAMIC LOADS ON UNDERWATER
ROBOT ARMS

CENTRE FOR NEWFOUNDLAND STUDIES

**TOTAL OF 10 PAGES ONLY
MAY BE XEROXED**

(Without Author's Permission)

CARLOS RIVERA



HYDRODYNAMIC LOADS ON UNDERWATER ROBOT ARMS

By

© Carlos Rivera, B. Eng.

A thesis submitted to the School of Graduate Studies
in partial fulfillment of the
requirements for the degree of
Master of Engineering

Faculty of Engineering and Applied Sciences
Memorial University of Newfoundland
March 1995

St. John's

Newfoundland

Canada



National Library
of Canada

Acquisitions and
Bibliographic Services Branch

395 Wellington Street
Ottawa, Ontario
K1A 0N4

Bibliothèque nationale
du Canada

Direction des acquisitions et
des services bibliographiques

395, rue Wellington
Ottawa (Ontario)
K1A 0N4

Your file Votre référence

Our file Notre référence

The author has granted an irrevocable non-exclusive licence allowing the National Library of Canada to reproduce, loan, distribute or sell copies of his/her thesis by any means and in any form or format, making this thesis available to interested persons.

L'auteur a accordé une licence irrévocable et non exclusive permettant à la Bibliothèque nationale du Canada de reproduire, prêter, distribuer ou vendre des copies de sa thèse de quelque manière et sous quelque forme que ce soit pour mettre des exemplaires de cette thèse à la disposition des personnes intéressées.

The author retains ownership of the copyright in his/her thesis. Neither the thesis nor substantial extracts from it may be printed or otherwise reproduced without his/her permission.

L'auteur conserve la propriété du droit d'auteur qui protège sa thèse. Ni la thèse ni des extraits substantiels de celle-ci ne doivent être imprimés ou autrement reproduits sans son autorisation.

ISBN 0-612-01912-8

Canada

Abstract

Computed Load and Sliding Mode control strategies for robots make use of the overall equations of motion. Unfortunately, for robots working in a marine environment, these equations do not provide an accurate control because of a lack of good hydrodynamics data.

The objective of the thesis is to incorporate the hydrodynamic loads, acting on robot arms working underwater, into the equations of motion. The thesis describes a two-link robot arm model and experimental setup designed for the purpose of gathering hydrodynamic data.

The thesis also describes the techniques used to analyze the obtained data. These include dimensional analysis and a neural network identification program.

Acknowledgements

I would like to express my gratitude and thanks to Dr. Michael Hinchey for his constant support and valuable guidance during the period of my studies in the Master's program, and in particular during the research part that led to the completion of this work.

I also extend my appreciation to the School of Graduate Studies and the Faculty of Engineering and Applied Sciences for the financial support I received.

I would like to thank Andrew Kuczora for his help beyond his duties in the data acquisition and processing, a crucial part of this work, and Humphrey Dyer and the rest of the people in Technical Services who helped me construct the experimental model.

I thank my wife Debbie for her unconditional support.

March 1995

Carlos Rivera

Contents

Abstract	ii
Acknowledgements	iii
List of Figures and Tables	vi
List of Symbols	vii
1. Introduction	1
1.1 Background	1
1.2 Scope and objectives	3
2. Literature Review	4
2.1 Background	4
2.2 AUV/ROV State of the art	6
2.3 Hydrodynamics loads on cylinders	11
2.3 Hydrodynamics loads on robot arms	24
2.4 Neural networks	28
3. Mathematical model of hydrodynamics loads on a robot arm	35
3.1 Analysis of a two-link planar revolute joint arm	36
3.2 Mechanical losses	52
3.3 The dynamic equations of motion	55

4. Wave tank experiment	62
4.1 Design of the two-link planar revolute joint arm model	62
4.2 Testing	66
4.3 Data acquisition and processing	67
4.4 Neural network system identification	71
5. Experimental and theoretical results	76
6. Conclusions	104
7. Recommendations	106
References	107
Appendix A. Flow charts of the neural network identification system	113
Appendix B. Programs Listing	127
Appendix C. Training Data	140

List of Figures

2-1a	Backlash compensating mechanism	8
2-1b	Pressure compensating system	8
2-2	The Jason ROV	9
2-3	Manipulator of the Jason ROV	10
2-4	Cylinders in tandem and side-by-side arrangement	16
2-5	Drag coefficients for cylinders with two free ends	18
2-6	Torque versus reduced velocity for accelerated motions	23
2-7	Stationary two link planar revolute joint arm	25
2-8	Two link arm model moving in three dimensions	26
2-9	Arm/body test configuration	28
2-10	Processing element of a neural network	31
2-11	A one hidden layer MLP in matrix notation	33
3-1	One-link planar arm model	37
3-2	Two-link revolute planar arm model	41
3-3	Force profile on link (case I)	44
3-4	Force profile on link (case II)	45
4-1	Experimental setup of a two-link underwater arm model	63
4-2	Driving section of the setup	64
4-3	Two-link underwater arm model	65
4-4	Neural Network with common middle layers	72
4-5	Neural Network with parallel middle layers	74
5-1 through 5-24	Data graphs	80-103
A-1 through A-10	Flow charts for the Neural Network Identification	116-126

List of Symbols

A_i, B_i	Coefficients in the velocity expression
C_D, C_M, C_a	Drag, Inertia and added mass coefficients
C_{m1}, C_{m2}	Centroid coordinate for the distribution of the drag/inertia forces
D	Link diameter / Relating to hydrodynamic drag as superscript
e	Error
f_a, f_b	Drag/inertia force along the links
H	Manipulator inertia tensor matrix
I	Inertia tensor / Relating to hydrodynamic inertia as superscript
i	Index for the link number
J_A, J_L	Jacobian matrices for angular and linear velocities respectively
k	Coefficient
L, L_c	Length of link / Location of the center of mass
M_i, N_i	Coefficients in the acceleration expression
m_i	Mass of links
Q_i	Generalized load
R_i, R_m, R_o, R_t	Inputs, outputs from the middle layer, output from the net and target outputs respectively
T	Total kinetic energy / Experimentally measured torque
u	Linear velocity of the link / Velocity of the carrier
W_i, W_o	Input and output weights
x, y	Denotes the x or y direction
Z, \hat{Z}	Output of the net and desired output
θ	Angular position
$\dot{\theta}$	Angular velocity
$\ddot{\theta}$	Angular acceleration
ν	Kinematic viscosity
ρ	Density
τ	Torques at the joints

Chapter 1

Introduction

1.1 Background

Although the oceans cover more than two thirds of the Earth's surface and are a vital part of the existence of Mankind, humans have not yet been able to fully explore their finite depths. Actually we now know more about outer space than we know about the oceans.

Modern robotics offers humanity a wide array of economically and socially sound benefits. Autonomous robots can potentially handle tasks in hostile or inaccessible environments, such as, in space, in nuclear reactors and underwater. Industrial robots have already assumed many hazardous, unpleasant or boring tasks, while simultaneously improving the productivity of factories in the industrialized world. Robot arms such as Canadarm have been successfully deployed in space. The ocean floor contains valuable minerals and fuels but the actual economic exploitation of these resources has been restricted by technological capabilities and the application of robots to underwater tasks has been very limited. Recent advances in underwater vehicle technology are helping to

change this situation.

Most of underwater vehicles are manually controlled. However, recently there has been a shift towards autonomous or digitally driven control. This is mainly because manual control has been found unsatisfactory for certain tasks. Most arms mounted on underwater vehicles operate at slow speeds, where the hydrodynamic forces are relatively small but not negligible (Farbrother and Stacey, 1993). However, the arms sometimes have to operate in the wake of a moving vehicle or be immersed in a current. In these cases the hydrodynamic loads on them can be considerable and unpredictable. The sudden change in the drag coefficients for a relatively small change in velocity makes the hydrodynamic loads very difficult to ascertain. These effects can bring instability to an automatically controlled vehicle. Therefore, arms operating in these conditions will require that control systems be robust and able to maintain acceptable performance levels in response to uncertainties (Farbrother and Stacey, 1993).

The control strategies used in robots can be divided in two main groups: conventional (classical) control techniques and supervisory control techniques. Some of the techniques in both groups can exhibit adaptive capabilities. By adaptive capabilities is meant the ability of the controller to accurately respond when faced with changes in the environment, which had not been anticipated or programmed (Westerman, 1991). The conventional control strategies include, among others, the computed load technique and the sliding mode. They are both based on the equations of motion and could be inaccurate for underwater applications because of uncertainties in the equations of motion. Good experimental data could be used to reduce such uncertainty.

Neural networks and fuzzy logic are considered supervisory control strategies. They try to mimic a human operator by picking set points and gains for classical strategies.

1.2 Scope and Objectives

The determination of hydrodynamics data is vital to perform an efficient control of the motion of robot arms in an underwater environment. Unfortunately very little data can be found in open literature. For this reason torque measurements have been conducted using the wave/towing tank facilities on single-link body configuration and on a two-link planar arm configuration. The measurements were conducted using steady translations and rotations. A neural network was used to provide a convenient fit to the torque data. In addition, a mathematical model based on the Morison's equation was developed for the hydrodynamics loads. More complex motions and geometry were avoided because even simpler cases are not fully understood.

Chapter 2

Literature Review

2.1 Background

A robot arm working under water is constantly under hydrodynamics loads, such as drag, hydrostatic restoring force, force due to the moorings and the force due to currents and waves (Muggeridge and Hinchey, 1991). The added mass effects would also play a substantial role in the power requirements of the arm (Baker and Sayer, 1990). In addition to underwater currents, the turbulence created by thrusters of the host vehicle itself or other passing vehicles, may affect greatly the dynamics of the arm (Rivera and Hinchey, 1992). In this case control strategies are bound to fail since the equations of motion lack good hydrodynamics data, and for complex configurations they are computationally expensive. In order to make control strategies work effectively underwater, a model of a robot arm would have to be fabricated and tested underwater. Then we would be able to find the data fit which is computationally least expensive and most robust.

The hydrodynamics of underwater vehicles or robot arms undergoing arbitrary, unsteady motions is very difficult to deal with analytically (Muggeridge and Hinchey, 1991). The major problem is the complex wakes set-up behind the body. Even steady motions are very difficult to treat analytically and the treatment relies heavily on experimental data. Most studies assume the flow to be quasi-steady, in other words, flows set up quickly and resemble steady flows. The quasi-steady approximation is perhaps acceptable for uniform or slowly varying motions of the arm but questionable for general arbitrary motions.

For steady flow wakes behind a body, much depends on the Reynolds number ($Re = u_\infty D / \nu$) (Slaouti and Stansby, 1992). Section 3 of the hydrodynamics text by Sarpkaya and Isaacson (1981) gives a good overview of this type of motion. At low Re the flow is viscosity dominated. At high Re , vortices (symmetric/asymmetric) shed downstream due to boundary layer separation, the flow cannot remain attached to the body as it moves into the adverse pressure gradient generally found there (Prandtl and Tietjens, 1934). Turbulence is a feature of fluid flow, not a property of the fluids themselves, and exhibit irregularity and randomness in time and space, diffusivity and rapid mixing, three-dimensional vorticity fluctuations, and dissipation of the kinetic energy of the turbulence by viscous shear stresses. It has also been observed that fluid particles in a turbulent flow travel as randomly moving fluid masses, which causes at any point in the flow, a rapid and irregular pulsation of velocity about a well-defined mean value. Turbulent boundary layers do not separate as easily as laminar boundary layers. The fluid in turbulent boundary layer is more energetic and can move farther into an adverse

pressure gradient. Bodies with turbulent boundary layers have smaller wakes and therefore less wake drag.

Most real flow problems can be solved, at best, only approximately by analytical or numerical methods. Thus, experiments are essential in verifying solutions, in suggesting which models are valid or in providing results that could not be obtained by theoretical analysis or numerical simulation (Szirtes, 1992).

All the above mentioned factors have to be considered in order to gain a better understanding of the hydrodynamics of underwater robot arms.

2.2 AUV/ROV State of the Art.^{1 2}

Papers in this area were reviewed with the purpose of gaining an understanding of the complexity of the task of deep ocean exploration, and the problems faced in the design and operation of such crafts; the hydrodynamic loads on arms happens to be one of the many.

Autonomous Underwater Vehicles, AUVs, are still in the early developmental stage (Zorpette, 1994) and the most advanced vehicles known today are the result of research recently unclassified by the military in several countries. Blidberg et al. (1991) give a good overview of the present state of the research in this area, which includes capabilities such as operational depth, mobility, autonomy, etc, along with a chronological development of these craft. The same paper outlines some of the non-military needs for the development of automated underwater technology, that are helping to promote a

¹AUV: Autonomous Underwater Vehicle

²ROV: Remotely Operated Vehicle

widespread use of these vehicles, and therefore the access to a more varied source of research resources.

Yoerger et al. (1991) describe in detail the design of the arm used on the JASON ROV, which has been successfully used in deep subsea exploration. It shows the ingenious design solutions applied to cope with the high pressure (approximately 9,000 psi for a depth of 6,000 meters) and extremely corrosive and electrically conductive environment, while at the same time exhibiting no backlash and low friction. The mechanism used to prevent backlash at the shoulder of the arm, a reducer with a system of pulleys, is shown in figure 2-1a. To ensure the needed stiffness, four parallel cable circuits are used on the output stage, two circuits on the intermediate stage and only one on the driver stage. Tensioning of the cable circuits is adjusted at the drive pinion. The pressure compensating system is shown in figure 2-1b. The manipulator is pressure compensated, all the parts run in an oil-filled encasement slightly above ambient pressure (9000 psi). The overpressure is maintained by spring-loaded bellows. Mineral oil was chosen which in addition to providing overpressure, lubrication and cooling allowed the researchers to visually examine the parts during testing. The JASON ROV and its arm are shown in figures 2-2 and 2-3 respectively.

Farbrother and Stacey (1993) review some of the aspects in designing ROVs with control in mind. The paper centers its attention on the problem of controlling the movement and positioning of the ROV itself, but does not make any reference to the control of the arm.

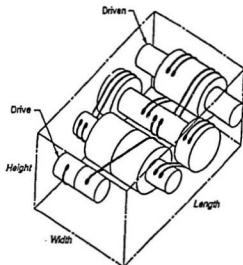


Figure 2-1a Backlash Prevention Reducer, Yoerger et al., 1991

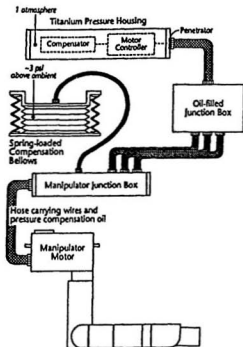


Figure 2-1b Manipulator's pressure Compensating System, Yoerger et al., 1991.

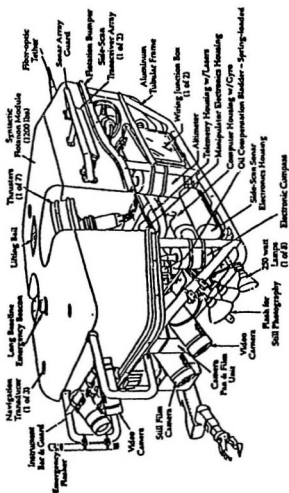


Figure 2-2 The JASON ROV, Yoerger et al. 1991.

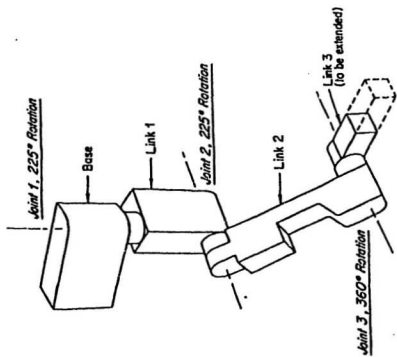


Figure 2-3 Manipulator of the JASON ROV, Yoerger et al. 1991.

2.3 Hydrodynamics Loads on Cylinders

In the present work we have used cylinders to model the links of an underwater robot arm, mainly because the case of hydrodynamic loads acting on cylinders has been extensively studied by many researchers. However the vast majority of these studies concern steady and oscillatory flows around cylinders of infinite length, although most practical applications have at least one free end, and very few have devoted effort to flows around cylinders with finite span. The case of arbitrary complex motions of finite span cylinders with two free ends like the arm in the present work has not been seriously researched. Therefore most of the data concerning hydrodynamic forces acting on cylinders are not applicable in this case.

Our model consists of two cylinders of finite span linked by a revolute joint. The three dimensionality of the cylinders with two free ends, plus their influence on each other, causes the hydrodynamic forces to differ from those found in the case of infinite cylinders or quasi two dimensional cylinders (end plates). Also, the specifics of the kinematics of the robot arms can cause different flow regimes to take place, even along the same link.

When a body moves through a fluid a force is exerted on the body by the fluid. The component of this force parallel to the free stream relative velocity is called drag, whereas the component perpendicular to the free stream velocity is called lift. Both pressure, p , and viscous shear, τ_v , contribute to the resultant forces. Theoretically, the drag and lift forces on a moving body could be calculated if we were to know the pressure and viscous stresses distribution over the entire surface of the body, equation 2-1 and 2-2.

$$\text{Drag} = \int (p \sin \theta + \tau_o \cos \theta) dA \quad 2-1$$

$$\text{Lift} = \int (p \cos \theta - \tau_o \sin \theta) dA \quad 2-2$$

Here θ is the polar angle from the centre of the cylinder to the point on the surface. Unfortunately it is extremely difficult to compute exactly the complete flow and pressure pattern over the entire relevant surface of most bodies. Equations 2-1 and 2-2, although formal, are of little practical value. In practice, for the most part, drag and lift are calculated using empirical or semi-empirical methods.

Morison's equation, equation 2-3, was developed to describe the horizontal wave force per unit length, f_y , acting on a vertical pile extending from the seabed to the ocean surface (Chakrabarti, 1987).

$$f_y = C_M \rho \frac{\pi}{4} D^2 \frac{\partial u_y}{\partial t} + C_D \frac{1}{2} \rho D |u_y| u_y \quad 2-3$$

Here C_M is the inertia coefficient, C_D is the drag coefficient, ρ is the density of the fluid, D the diameter of the cylinder and u_y the component of the velocity normal to the cylinder's axis. Usually C_M and C_D are functions of the Reynolds number, defined earlier, and the Keulegan-Carpenter dimensionless parameter, $KC = u_o T / D$, where T is the period of the wave. The equation consists of two terms, inertia and drag. A particle of water passing around a circular cylinder first accelerates and then decelerates, and this applies a force on the cylinder. This force is described by the first term in equation 2-3. The

principal cause for drag is the existence of a low pressure region on the downstream side of the cylinder and a higher pressure zone on the upstream side (Prandtl and Tietjens, 1934).

Morison's equation is semi-empirical and its application to a complex time dependent separated flow is questionable. However, attempts to derive other formulations to better describe the phenomena have been unsatisfactory. Some proposals have been made to improve the existing equation (Sarpkaya and Isaacson, 1981) by adding higher harmonic terms. Other more complex solutions have been attempted (Nam, 1990). But overall the original Morison's equation has been reliable in predicting fluid forces on small members. The equation can be extended to the computation of fluid forces on inclined cylinders by writing it in terms of the normal velocity and acceleration vectors (Chakrabarti, 1987, Bin and Yu-Cheng, 1991 and Otsuka and Ikeda, 1991).

The Morison's equation was developed to match the peak forces due to a separated flow. However, for attached flows the forces are not well described by Morison's equation (Anartuk et al., 1992). The essence of some new models (Anartuk et al., 1992 and Sarpkaya, 1991) is that the mean rate of the work done by the drag or damping force must be equal to the rate of energy dissipation. Each of these models however assumes that the flow remains attached at all times which makes the range of its use rather narrow.

A potential flow model (Chew et al., 1992) has actually validated the much criticized Morison's equation for unsteady flow. The method is based on a two dimensional potential flow model that simulates the effect of flow separation in unsteady flow by placing surface sources with time dependent strength and angular positions on the

rear wetted surface of the body and downstream sinks in the flow to form a closed wake model. Then the unsteady Bernoulli equation is used to obtain the time dependent pressure. The in-line force equation obtained by this model is comprised of uncoupled drag and inertia terms. With some simplifications the equation reduces to the classical Morison's equation. This work supports the applicability of the Morison's equation to unsteady separated flows. The cases considered showed small variations of the drag and inertia coefficients over a cycle. This is why Morison's equation with mean coefficients predicts the in-line force rather precisely. This method, however, did not take the surface roughness in consideration, a factor that affects greatly the drag force (Sarpkaya, 1990).

Since Morison's equation was proposed in 1950, it has been a challenge to find a correlation for the drag and inertia coefficients. In fact, satisfactory correlations of with the relevant dimensionless parameters have not been achieved. Data correlations to date usually plot each dynamic coefficient versus one of the dimensionless parameters ignoring the others (Makhortikh and Shcheglova, 1990 and Shcheglova and Makhortikh, 1988). This has led to scatter correlations (Horton et al., 1992, and Rao et al., 1992). Generally flows around circular cylinders are turbulent and wakes have a three dimensional unsteady character (Slaouti and Stansby, 1992). There is no general turbulent model to incorporate into a numerical simulation of unsteady separated flows and the limitations of computing power will not allow the direct three dimensional numerical solution of the Navier-Stokes equations in the near future (Slaouti and Stansby, 1992 and Sarpkaya, 1991). At low Reynolds numbers, the flow and forces on a cylinder may be reasonably predicted by two dimensional laminar computations (Kawamura et al., 1986),

although even here, the flows are known to contain some three dimensional characteristics (Tatsuno, 1989, and Slaouti and Stansby, 1992).

There have been a few numerical studies of two cylinders in side-by-side and tandem arrangements using the random vortex method (Sin, 1987). This method is believed to be versatile and efficient, not exhibiting some of the numerical diffusion and dissipation problems associated with fixed mesh schemes. It has been observed that for the side-by-side arrangement (Sin, 1987), for large spacings ($T/D > 3.5$), where T is the distance between the two cylinders and D their equivalent diameter (figure 2-4), the interaction between the two cylinders is negligible, and the two cylinders form their own vortex streets independently. Spacings in the range of $2 < T/D < 3.5$ causes the cylinders to produce vortex shedding in anti-phase. Spacings of $1.2 < T/D < 2$ results in strong interaction, producing one narrow near-wake and a wide near-wake. The two near-wakes occasionally switch over and a large scale vortex street is formed further downstream. For spacings of $1 < T/D < 1.2$ the flow velocity in the gap is small and a large formation region occurs, resulting in the formation of a large scale vortex street. Sources (Slaouti and Stansby, 1992 and Zdravkovich et al., 1989) show drag coefficients and Strouhal numbers for each cylinder for different spacing ratios. The repulsive force between the two cylinders, as expected, decreases gradually with increasing spacing ratio T/D , and disappears when $T/D > 3$.

In the tandem arrangement, source (Slaouti and Stansby, 1992) found that a critical spacing exists which divides the flow regime into two categories. For spacing ratios of $T/D > 3.8$ each cylinder produces a vortex wake and for $T/D < 3.4$ vortex shedding

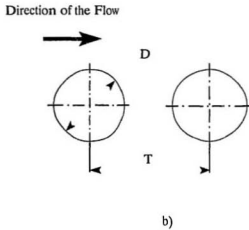
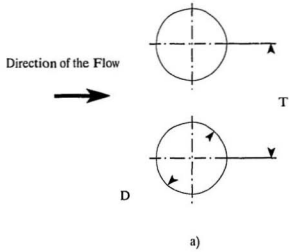


Figure 2-4 Cylinders in Side-by-Side, a), and Tandem Arrangements, b).

does not occur between the two cylinders. At spacing ratios of $1 < T/D < 1.1$ the two bodies behave like a single slender body, the separated shear layers of the upstream body enclose the downstream body and a vortex street forms downstream of the rear body. C_D shows a sudden increase as T/D exceeds the critical value.

In most practical applications, like in our model, there is at least one free end, a case which has attracted little attention (Zdravkovich et al., 1989). For cylinders with length to diameter ratio $L/D > 6$, it has been observed (Zdravkovich et al., 1989) that vortex shedding occurs along most of the span except near the free end. Flow visualization (Zdravkovich et al., 1989) has demonstrated that the interaction of the vortex shedding and the free end was extremely complex. Also "eyes" were visualized near the surface near the free end. Each "eye" is thought to be associated with low pressure which is responsible for an increase in the local drag coefficient. For $L/D = 5$ in phase pressure fluctuations have been reported (Yeung et al., 1993) on the two sides of the cylinder. Arc shaped vortices have been observed being formed behind short cylinders. The change-over from an alternate to a symmetric vortex street occurred near $L/D = 2.5$. A short cylinder with two free ends has two interacting side flows which inhibit the vortex shedding (Eckerle and Awad, 1991). A short cylinder with two hemispherical ends approximates the shape of an ROV (Baker and Sayer, 1990). Reduction of L/D decreases the drag coefficient (figure 2-5). Zdravkovich et al. (1989) argue that the explanation should be sought in the venting of a near wake which occurs behind a bluff body, i.e. an inflow of the fluid into the near wake space on its way around the cylinder's ends. Hence the pressure over the back side of the body would rise resulting in a smaller drag. It should

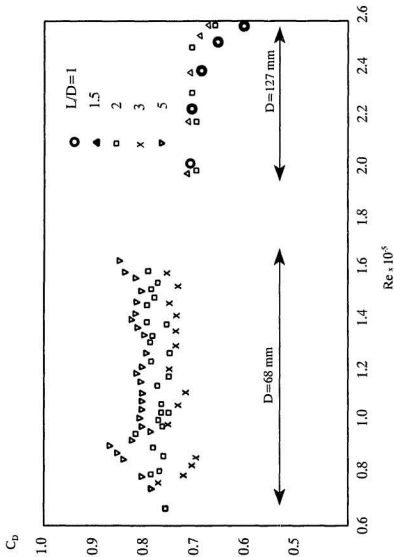


Figure 2-5 Drag coefficient variation with Reynolds number and L/D , Zdravkovich et al. (1989).

be pointed out that it takes some time for the inflow to turn and reach the near wake. The result is a low pressure region near the free ends causing a high local drag coefficient. Zdravkovich et al. (1989) observed that the separated shear layers from sharp edged circular ends form two counter-rotating swirling vortices, which separate from the free ends where the flow around the rest of the cylinder does and are carried downstream as streamwise vortex pair. The effect of the inflow on the near wake along the span does not merely increase the base pressure but also displaces the vortex formation region further downstream and widens the separated shear layers before roll-up into vortices (Nakamura et al., 1992). This contributes to a reduction of the drag coefficient and causes a decrease in frequency vortex shedding. In addition the Strouhal number measured behind finite cylinders is always smaller than behind infinite cylinders. The rate of fall of the drag coefficient becomes negligible for $L/D < 6$. This indicates that with further reduction of L/D the drag becomes governed by the shape of the two free ends. When using hemispherical ends the drag can be reduced until $L/D = 1$ and the cylinder becomes an sphere (Zdravkovich et al., 1989).

The effect of the Reynolds number is similar to that found on cylinders of infinite length. However, the separation lines are displaced gradually towards the stagnation point line as L/D decreases, and eventually becomes bow-shaped for $L/D = 2$. The concept of a universal Strouhal number (Zdravkovich et al., 1989 and Nakamura et al., 1992) which is based on data from infinite cylinders is not applicable in regions of three dimensional flows such as near the ends of a finite cylinder (Ko et al., 1987). The three dimensional effects on the drag coefficient of a finite length circular cylinder is quite

similar to that in steady flow (Nakamura et al. , 1992). The values of the added mass coefficient , C_m , for a finite span cylinder are about equal to those for quasi two dimensional circular cylinders for Keulegan-Carpenter numbers $KC \leq 8$ and larger than those for $KC > 8$ (Sarpkaya and Isaacson, 1981). The values of the added mass coefficient for infinite two dimensional cylinders decrease in the interval $8 < KC < 25$, but finite cylinders do not exhibit this behaviour. The lift coefficients are also smaller for finite span cylinders (Nakamura et al., 1992).

Unlike infinite two dimensional cylinders, the problem of finite span cylinders placed in a uniform cross flow has not been studied extensively. Our understanding of the vortex shedding phenomenon and the associated flow induced unsteady forces is rather poor. This is partially due to the complexity of the separated flow, its three dimensional nature and its interaction with the wake flow and partly because of a lack of reliable techniques to resolve the unsteady forces induced on finite span cylinders (Baban et al., 1989).

In spite of the interest in unsteady flow past a bluff body and many experimental measurements of the unsteady flow induced forces, there are very few numerical works in this area due to its complexity. Analytical solutions for separated time dependent flows are not yet possible even for relatively idealized situations (Kiya and Tamura, 1989).

When a two dimensional cylinder is placed in a cross flow, alternate vortex shedding from both sides of the cylinder induce fluctuating lift and drag forces (Baban et al., 1989, Blevins, 1990, Sarpkaya et al., 1981 and Sarpkaya 1991). The frequency of vortex shedding is given in terms of the Strouhal number: $S = nD/u_\infty$, where n is the

frequency of vortex shedding from one side of the cylinder. D is the diameter of the cylinder and u_0 is the free stream velocity. The Strouhal number depends in turn on the Reynolds number. If the Reynolds number is in the subcritical range the frequency of the drag is about twice that of the vortex shedding (Baban et al., 1989). It has been observed that the fluctuating drag signal does not correlate well with the vortex shedding frequency. It has been shown that the complex, three dimensional flow which exists behind the cylinder inhibits the periodic shedding of vortices. This effect is variable along the cylinder's span (Sin, 1987, and Niemann and Hoelscher, 1990).

A large volume of literature deals with fluctuating forces and associated vortex shedding from bluff bodies subjected to steady ambient flow. Numerous computational studies have been performed on flow about circular cylinders attempting to predict the Strouhal number in steady ambient flow and the shape and growth of the wake region in impulsively started flow (Gopalkrishnan et al., 1992 and Wang and Dalton, 1991). The complete Navier - Stokes equations in vorticity/stream function form have been solved (Burdic, 1990) using a combination of second and fourth order compact finite difference schemes. Short time symmetric - wake solutions for Reynolds numbers of 300, 550 and 1000 were obtained showing good agreement with visualization results for both vortex size and center position (West and Apelt, 1990).

The evolution of the drag coefficient does not depend significantly on the reduced velocity, $u_0 t / D$, where u_0 is the linear velocity or free stream velocity, t is the time and D the diameter of the cylinder beyond the period of constant acceleration, figure 2-6. A drag overshoot occurs between $u_0 t / D \approx 4$ and $u_0 t / D \approx 5$ (at a relative distance covered in

approximately half the vortex shedding period). The drag overshoot occurs before the vortices exhibit noticeable asymmetry. The reasons for high local drag could be the following (Sarpkaya, 1991) : During the initial and symmetric development of vortices (for $u_o t / D < 4$), the vorticity rapidly accumulates in the wake. The symmetric vortices grow to sizes considerably larger than those found in later stages of the motion where the vortices shed alternately. But, this is not enough to explain the drag overshoot. Also, during the early stages of motion the vorticity flux is expected to be considerably larger than the cross wake transfer of oppositely signed vorticity. The vortices grow and exhibit three dimensionality. The combination of the above mentioned factors contributes to the rapid rise and fall of the drag coefficient at or near $u_o t / D \approx 4.5$ (Yeung et al., 1993).

Cylinders may be classified as semi-streamlined bodies where the position of separation is varying depending on the free stream velocity and flow profile, turbulence of the free stream, geometry and the roughness of the body's surface (Niemann and Hoelscher, 1990). The flow around a circular cylinder depends on Reynolds number, since the state of the boundary layer may be either laminar or partly turbulent (Badr et al., 1989). In turbulent conditions, additional energy is fed to the boundary layer by turbulent momentum exchange and hence it gains additional capability of overcoming the adverse pressure gradient behind the pressure minimum, producing a smaller width of the wake, recovery of the wake pressure and smaller drag. Most researchers agree about these features but the steps by which the transition from laminar to turbulent occurs is not completely understood (Niemann and Hoelscher, 1990 and Sarpkaya, 1991). In the case of a cylinder oscillating in the presence of a steady current, the flow may be characterized

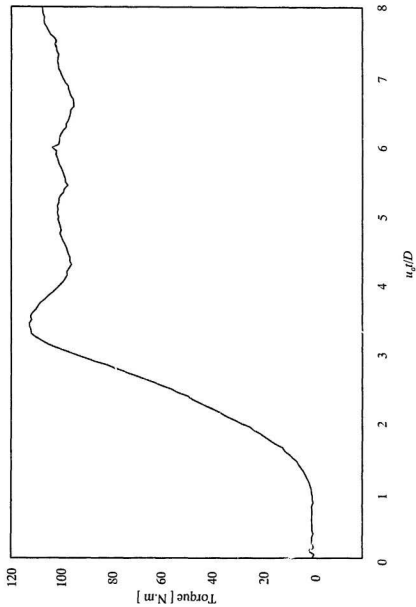


Figure 2-6 Torque at the joint versus reduced velocity, accelerated from $u=0$ ($\theta = 0$)

by three non-dimensional parameters, the reduced velocity, the Reynolds number and the amplitude parameter (Badr et al., 1989).

2.4 Hydrodynamics Loads on Robot Arms

Very little has been found in the literature regarding this specific topic, the central part of this thesis. Most of the papers reviewed deal with hydrodynamics and control of ROVs, or with hydrodynamic forces on offshore structures. Only three relevant references have been found, Fukuda and Hara (1989), Liceaga-Castro et al. (1991) and Lee (1993).

Liceaga-Castro et al (1991) proposed a mathematical model based on Morison's equation, which uses drag and inertia (added mass) coefficients determined for infinite circular cylinders. In the case of the added mass coefficients, a constant value of $C\alpha=1.8$ is used. The manipulator model described is a two-link planar arm with two degree of freedom, figure 2-7: the two joints rotate in one plane and there is no translation. The effects that one link has on the other were not considered. The hydrodynamic loads on the model were incorporated into the derivations of the equations of motion using the Newton-Euler method. In this thesis it was decided to use the Lagrange formulation.

Fukuda and Hara (1989) (in Japanese) use a simplified mathematical model of the hydrodynamic forces incorporated into an adaptive controller for an underwater robotic manipulator. The model states that the equivalent drag force acts at the midspan of the link. The physical model tested is a two-link arm with joints rotating in perpendicular planes, figure 2-8, the rotation of the first joint occurs along the axis of the first link. A translation of the paper was unavailable but much could be inferred from the equations. The third source (Lee, 1993) is a video demonstration of a one-link revolute. An adaptive

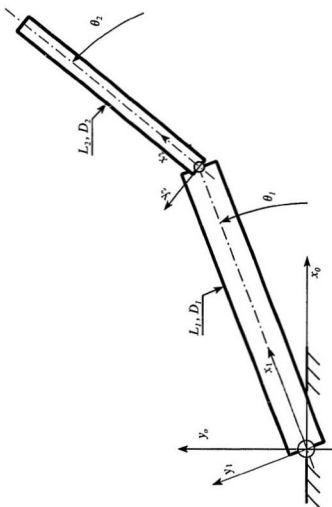


Figure 2-7 Two-Link Planar Revolute Arm Model, Liceaga-Castro et al. (1993)

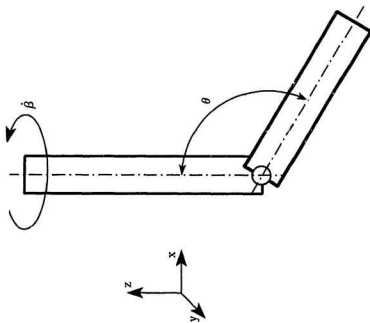


Figure 2-8 Two-Link Arm model moving in three dimensions, Fukuda and Hara (1988)

controller used was tested for angular positioning of the link. The demonstration lasted barely few seconds and only mentions that research is under way.

Rivera and Hinchey (1992) conducted experiments on an arm/body configuration (figure 2-9) which consisted of a spherical body, 0.25 m in diameter, with a box cross-section single link horizontal arm fixed to the body and 0.25 m long and 0.05 m wide. During tests the arm was position 1 m below the water surface in the MUN wave/towing tank facility; the tank itself being approximately 2 m deep. The motion of the carriage was used to generate steady translation and a DC motor was used to generate steady rotation. Torque data were obtained for various combinations of steady translation and rotation. Tests showed that the hydrodynamics forces acting on the arm behave randomly when the arm is positioned downstream from the body: for the combination shown in figure 2-9 (steady translation and no rotation) the torque measured read sometimes counterclockwise and others clockwise.

2.4 Neural Networks System Identification

The environment in which ROVs and AUVs work emphasize the requirement that control systems be extremely robust and capable of maintaining acceptable performance levels in the face of parametric uncertainties and unmodelled disturbances (Farbrother and Stacey, 1993). Recent advances in control strategies for ROVs and AUVs include not only neural nets, but there is an adaptive element in almost every new proposal (i.e. Pap et al., 1991, Zomaya and Tarek, 1993 and Westerman, 1991). But maintaining an on-line adaptive capability (i.e. after the neural network has been trained) is computationally expensive for present practical use (Farbrother and Stacey, 1993). Westerman (1991) has

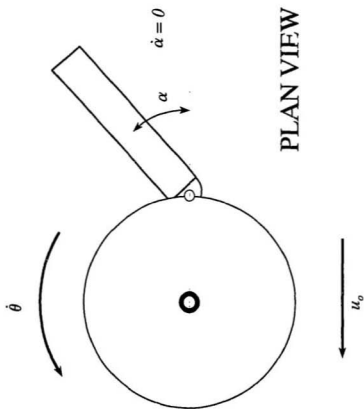


Figure 2-9 Arm/Body Test Configuration

been able to maintain an on-line adaptive controller for only two degrees of freedom of five degree of freedom arm: hardware limitations have been the source of this shortcoming. Zomaya and Tarek (1993) have used decentralized neuro-adaptive controllers (a controller per joint) for the control of some industrial robots. Pap et al. (1991) describe a very similar procedure for underwater robotic operations.

Artificial neural networks have biologically inspired architectures, but it would be a misconception to think that neural nets mimic accurately brain activity. Most of the working applications of neural nets today have more in common with statistics and data manipulation than with the simulation of grey matter (Westerman, 1991). Basically neural networks are a means of correlating data using multiple highly interconnected processing elements. The elements form a transfer function that maps input data to output data (Caudill, 1988). Neural nets do not need specific mathematical models correlating the input data to output data. They are able to come up with a relationship between the input variables and the output. A network can be trained by presenting it with known and reliable input/output samples, adapting themselves to map one to the other. After a sufficient number of training cycles, the network is able to generalize and produces a best estimate output, with a corresponding measure of certainty, in response to some new data. Neural networks will exhibit different properties depending on how they learn and train. A way of training a network is to present input samples with corresponding outputs (Zomaya and Nabhan, 1993). For each sample set, the network reads the input and estimates the output. It then compares its estimate with the correct response, using the error to adjust the weights in the processing elements. This is called supervised learning.

It tries to teach the network the right answer for any corresponding input during the training phase. From the above we can conclude that it is important to train the net with a "good" sample set. Determining what a good sample set of inputs and outputs is, for a given neural network, turns out to be a most difficult issue. A net may pay attention to relations in the data sample that may seem unimportant to people. If a network is undertrained, it will not yield reliable responses. If, on the other hand, it is overtrained, it just memorizes the taught cases and does not acquire the ability to generalize if posed with new data.

A network able to generalize can interpolate between cases found in the training sets. In this case what the neural network really does is to classify data: it is a way of matching signals to learned patterns. Neural nets can also generate complex signals with relative ease, which finds room in applications such as speech recognition and synthesis, and robotic control, (Craig, 1988, Kawato et al., 1988, Miyamoto et al., 1988 and Pap et al., 1993). Another advantage of neural nets is the ability to find answers in spite of incomplete and imprecise available data. Neural networks have also been used to develop adaptive control systems and we intend to use it to analyze the obtained data.

A neural network is made up of simple, highly interconnected processing elements, which respond in parallel to inputs presented in a dynamic, self-organizing way. Certain knowledge is contained within the network in the way the processing elements are connected and the weighting assigned to each neuron input. By itself, a single processing element, figure 2-10, is relatively useless: it is the interconnection of many that works. The processing elements are organized in layers and connected in different ways to

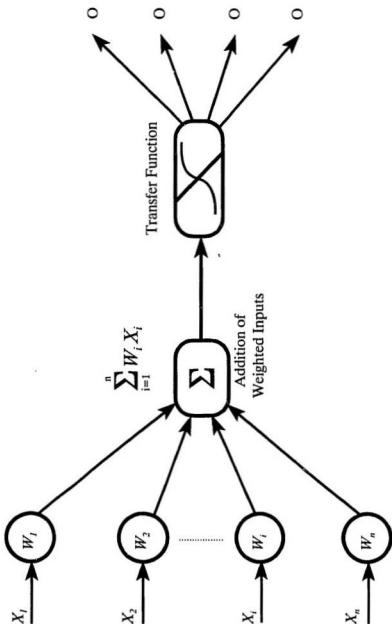


Figure 2-10 The processing element in a neural network

provide for the different learning dynamics for solving different problems. The connection weights are about the only thing that changes in a neural net as new data becomes available and thus provides for its adaptability. The weights vary in order to respond to data correlation. They are like the coefficients of a multi-variable system of equations, evolving to fit the data no matter how complex. It is possible that the transfer function be made variable in order to increase the learning speed, but this is still a matter of research. In the scope of this thesis we will use a type of architecture known as feedforward architecture. The activity flows only in the forward direction, originating in the input layer. In conjunction with this scheme we will use a back propagation learning algorithm. In this type of supervised learning, the desired output must be provided along with the input.

Sørensen (1993) describes a multi-layer perceptron system able to perform multidimensional curve-fitting in a multi-variable dynamic process. The neural network in question, figure 2-11, contains an input layer, a hidden layer with a sufficient number of non-linear neuron squashing functions including offsets, and an output layer with linear neuron functions. In this case W_1 is a matrix representing the weights between the input layer and the hidden layer, the "1" input provides the necessary offset. The matrix W_2 represents the weights between the hidden layer and the output layer and F represents the neural function, a tanh function for all elements. The error e , which represents the mismatch between Z , the desired output, and \hat{Z} , the output from the net, is used in the Back Propagation Error Algorithm, widely described in the literature on the subject. Sørensen (1993) extracts a so called Gain Matrix from a trained multi-layer perceptron,

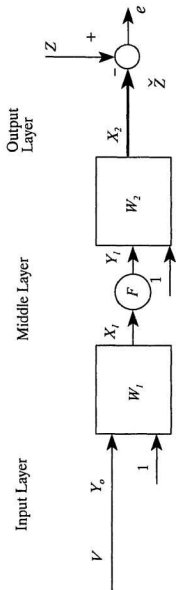


Figure 2-11 A one hidden layer MLP in matrix notation, Sørensen, 1993.

which is the derivative of the output vector, \mathcal{Z} , to the input vector of the net, V . This allows a trained multi-layer perceptron to work as an identification parameter routine.

Chapter 3

Mathematical Model of Hydrodynamic Loads on a Robot Arm

In this chapter a mathematical model of a planar two-link revolute joint robot arm is developed. The hydrodynamic torques were developed based on Morison's equation and dimensional analysis. The hydrodynamic model and the dissipating forces were then incorporated into the equations of motion of the two-link arm. The model is not expected to perform accurately, due to a lack of hydrodynamic data for cylinders with two free ends moving randomly in the plane and the effects of one cylinder on the other. The model is useful however in identifying the dimensional and dimensionless parameters that affect the joint torques, and in what measure they do so. These parameters constitute one of the input sets tried in the neural network described in chapter 5.

3.1 Analysis of a Two-Link Planar Revolute Joint Arm

Applying dimensional analysis (Sharp et al. 1992) to the one-link configuration undergoing steady translations and rotations shown in figure 3-1, we obtain a function for the torque depending on the independent parameters that influence its determination:

$$\tau^D = \phi (u_y, \dot{\theta}, \theta, L, D, \rho, \nu) \quad 3-1-1$$

where:

L - Length of the link	[m]
D - Diameter of the link	[m]
u_r - Normal velocity ($u_y = u_o \cos \theta$)	[m/sec]
u_o - Translational velocity of the base	[m/sec]
τ^D - Torque at the joint	[N.m]
ρ - Density of the fluid	[Kg/m ³]
ν - Kinematic viscosity of the fluid	[m ² /sec]
θ - Angle between the link and u_o	[radians]
$\dot{\theta}$ - Rotational velocity	[rad/sec]

As a first case we analyze the drag force on the single link when the translational velocity u_o is constant and the rotational velocity $\dot{\theta}$ equals zero. In this case the torque at the joint, due to the drag force on the link, may be expressed through the following functional equation:

$$\tau^D = \phi (\rho, \nu, u_o \cos \theta, D, L, \theta) \quad 3-1-2$$

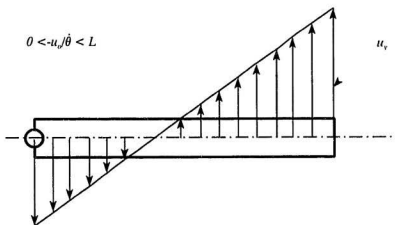
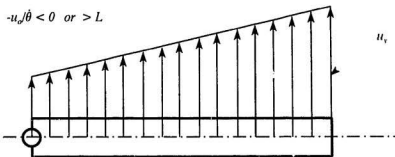
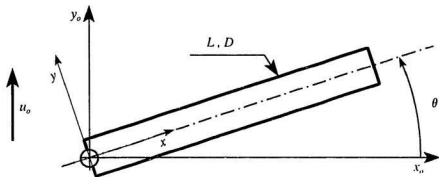


Figure 3-1 One-Link Planar Arm Model (Velocity Profile)

Using dimensional analysis the above equation can be reduced to a function of dimensionless parameters.

	u_0	L	τ^D	ρ	D	ν
L	1	1	2	-3	1	2
T	-1	0	-2	0	0	-1
M	0	0	1	1	0	0
π_1	1	0	0	0	1	-1
π_2	0	1	0	0	-1	0
π_3	0	0	1	-1	-1	-2

Compounding the pi terms gives:

$$\frac{\tau^D}{\rho L^2 D (u_0 \cos \theta)^2} = \phi \left(\frac{u_0 \cos \theta D}{\nu}, \frac{L}{D} \right) \quad 3-1-3$$

Applying Morison's equation to this case a similar expression is obtained for the torque at the joint:

$$\tau^D = \frac{1}{4} \rho D C_D L^2 u_0^2 \cos^2 \theta \quad 3-1-4$$

In this case the drag coefficient C_D , the term in the right hand side of equation 3-1-3, is a function of the Reynolds number and the L/D parameter and is constant along the link, except near the free ends.

In a second case, where the translational velocity is zero and the rotational velocity is constant, dimensional analysis yields the following functional equation after

compounding:

$$\frac{\tau^D}{\rho D L^4 \dot{\theta}^2} = \phi \left(\frac{\dot{\theta} L^2}{v}, \frac{L}{D} \right) \quad 3-1-5$$

Here dimensional analysis yields the so called rotational Reynolds number, the first term inside the parentheses in equation 3-1-5 (Oldshue, 1983); the conventional Reynolds number would be different along the length of the link. Once again applying Morison's equation and integrating along the link gives:

$$\tau^D = \frac{1}{8} \rho D \dot{\theta}^2 L^4 \phi \left(\frac{\dot{\theta} L^2}{v}, \frac{L}{D} \right) \quad 3-1-6$$

In this case the drag coefficient depends on the dimensionless parameters inside the parentheses.

A third more general case involves simultaneous rotation and translation. The significant functional equations obtained from dimensional analysis are:

$$\frac{\tau^D}{\rho D u_o^2 \cos^2 \theta L^2} = \phi \left(\frac{u_o \cos \theta D}{v}, \frac{\dot{\theta} L}{u_o \cos \theta}, \frac{L}{D} \right) \quad 3-1-7$$

$$\frac{\tau^D}{\rho D \dot{\theta}^2 L^4} = \phi \left(\frac{\dot{\theta} L^2}{v}, \frac{\dot{\theta} L}{u_o \cos \theta}, \frac{L}{D} \right) \quad 3-1-8$$

Following is an attempt to generalize the case of a revolute multiple link manipulator moving in the plane by applying Morison's equation (figure 3-2). The left hand side term in equation 3-1-7 or 3-1-8 constitute the drag coefficient.

The vertical and horizontal velocity distribution along a link i can be written as:

$$u_{yi}(x_i) = x_i \sum_{j=1}^i \dot{\theta}_j + \sum_{j=1}^{i-1} \dot{\theta}_j \left[\sum_{q=j}^{i-1} L_q \cos \left(\sum_{p=q+1}^i \theta_p \right) \right] + u_0 \cos \left(\sum_{j=1}^i \theta_j \right) \quad 3-1-9$$

$$u_{xi} = \sum_{j=1}^{i-1} \dot{\theta}_j \left[\sum_{q=j}^{i-1} L_q \sin \left(\sum_{p=q+1}^i \theta_p \right) \right] + u_0 \sin \left(\sum_{j=1}^i \theta_j \right) \quad 3-1-10$$

In the above equations x_i and y_i denote the local coordinate system, x_i equals zero at the joint i and L_i at the joint $i+1$. Equation (3-1-10) is of the type $f(x_i) = A_i x_i + B_i$, where A_i is equal to the sum of all angular velocities preceding link i , including the angular velocity of link i , and B_i is the sum of the second and third terms in equation (3-1-10). j , p and q are counters. The coefficients A_i and B_i can be found from:

$$A_i = \sum_{j=1}^i \dot{\theta}_j \quad 3-1-11$$

$$B_i = \sum_{j=1}^{i-1} \dot{\theta}_j \left[\sum_{q=j}^{i-1} L_q \cos \left(\sum_{p=q+1}^i \theta_p \right) \right] + u_0 \cos \left(\sum_{j=1}^i \theta_j \right) \quad 3-1-12$$

The joint displacements $\theta_i(t)$ and the translational velocity of the base are functions of time t . In the scope of this thesis only steady translations and rotations were tried, but even at constant translational velocity ($u_0(t) = \text{constant}$) and constant rotational velocity ($\dot{\theta}_i(t) = \text{constant}$), accelerations exist since the velocities $u_{yi}(x_i, t)$ and $u_{xi}(t)$ also depend on the configuration of the arm. The velocities and accelerations are used to calculate the drag and inertia terms in Morison's equation.

The following expressions compute the accelerations in the y , and x , directions:

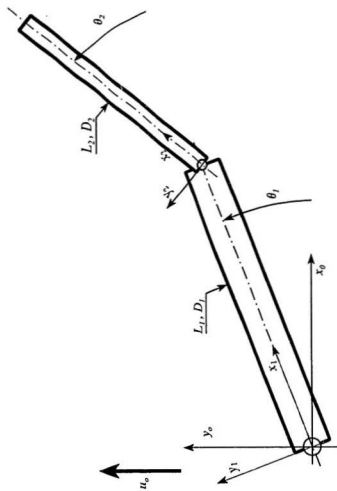


Figure 3-2 Two-Link Planar Revolute Arm Model

$$\left. \begin{aligned} \dot{u}_{yi} = \frac{\partial u_{yi}}{\partial t} = x_i \sum_{j=1}^i \dot{\theta}_j + \left[\sum_{j=1}^{i-1} \dot{\theta}_j \left(\sum_{q=j}^{i-1} L_q \cos \left(\sum_{p=j+1}^i \theta_p \right) \right) \right. \\ \left. - \sum_{j=1}^{i-1} \dot{\theta}_j \left(\sum_{q=j}^{i-1} L_q \sum_{p=q+1}^i \dot{\theta}_p \sin \left(\sum_{p=j+1}^i \theta_p \right) \right) \right] \\ + \left[\dot{u}_o \cos \left(\sum_{j=1}^i \theta_j \right) - u_o \sum_{j=1}^i \dot{\theta}_j \sin \left(\sum_{j=1}^i \theta_j \right) \right] \end{aligned} \right\} \quad 3-1-13$$

$$\left. \begin{aligned} \dot{u}_{xi} = \frac{\partial u_{xi}}{\partial t} = \sum_{j=1}^{i-1} \dot{\theta}_j \left(\sum_{q=1}^{i-1} L_q \sin \left(\sum_{p=q+1}^i \theta_p \right) \right) \\ + \sum_{j=1}^{i-1} \dot{\theta}_j \left(\sum_{q=1}^{i-1} L_q \sum_{p=q+1}^i \dot{\theta}_p \cos \left(\sum_{p=q+1}^i \theta_p \right) \right) \\ + \dot{u}_o \sin \left(\sum_{j=1}^i \theta_j \right) + u_o \sum_{j=1}^i \dot{\theta}_j \cos \left(\sum_{j=1}^i \theta_j \right) \end{aligned} \right\} \quad 3-1-14$$

In order to find the drag component of the force acting along the link i , we must integrate the first term of Morison's equation from 0 to L_p . However the solution of the integral of the expression does not have a common closed form for every configuration of the arm.

In the case where $-B_i/A_i \leq 0$ and $-B_i/A_i \geq L_i$, it is sufficient to have one interval for the integration from 0 to L_i . However if $0 < -B_i/A_i < L_i$ then two integration intervals are needed. The integration intervals are from 0 to $-B_i/A_i$ and from $-B_i/A_i$ to L_i . If $-B_i/A_i \leq 0$ or $-B_i/A_i \geq L_i$ (case I, figure 3-4) then:

$$f_{ayi}^D = \frac{1}{2} \rho D_i C_{Dyi} \operatorname{sgn}(u_{yi}(L_i)) \int_0^{L_i} (A_i x_i + B_i)^2 dx_i \quad 3-1-15$$

$$f_{ayi}^D = \frac{1}{2} \rho D_i C_{Dyi} \operatorname{sgn}(u_{yi}(L_i)) \left[\frac{(A_i L_i + B_i)^3}{3A_i} - \frac{B_i^3}{3A_i} \right] \quad 3-1-16$$

$$f_{byi}^D = 0 \quad 3-1-17$$

If $-B_i/A_i > 0$ and $-B_i/A_i < L_i$ (case II, figure 3-4) then:

$$f_{ayi}^D = \frac{1}{2} \rho D_i C_{Dyi} \operatorname{sgn}(-u_{yi}(L_i)) \int_0^{-\frac{B_i}{A_i}} (A_i x_i + B_i)^2 dx_i \quad 3-1-18$$

$$f_{ayi}^D = \frac{1}{2} \rho D_i C_{Dyi} \operatorname{sgn}(-u_{yi}(L_i)) \left[-\frac{B_i^3}{3A_i} \right] \quad 3-1-19$$

$$f_{byi}^D = \frac{1}{2} \rho D_i C_{Dyi} \operatorname{sgn}(u_{yi}(L_i)) \int_{-\frac{B_i}{A_i}}^{L_i} (A_i x_i + B_i)^2 dx_i \quad 3-1-20$$

$$f_{byi}^D = \frac{1}{2} \rho D_i C_{Dyi} \operatorname{sgn}(u_{yi}(L_i)) \left[\frac{(A_i L_i + B_i)^3}{3A_i} \right] \quad 3-1-21$$

The torque on joint j caused by the y , drag component of the hydrodynamic force on link i by u_{yi} can be determined from the following expression:

$$\tau_{i,j}^{Dy} = \left[C_{ai}^D + \sum_{q=j}^{i-1} L_q \cos \left(\sum_{p=q+1}^i \theta_p \right) \right] f_{ayi}^D + \left[C_{bi}^D + \sum_{q=j}^{i-1} L_q \cos \left(\sum_{p=q+1}^i \theta_p \right) \right] f_{byi}^D \quad 3-1-22$$

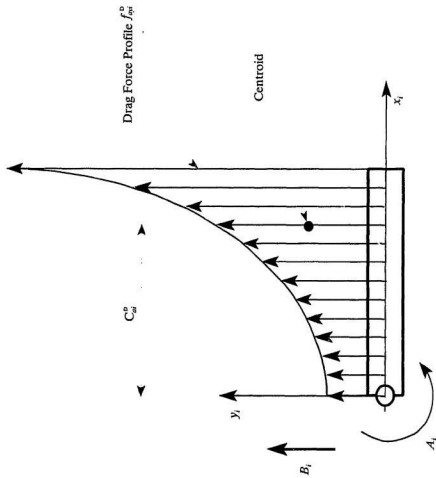


Figure 3-3 Force Profile of Link i of a Planar Revolute Arm (Case I)

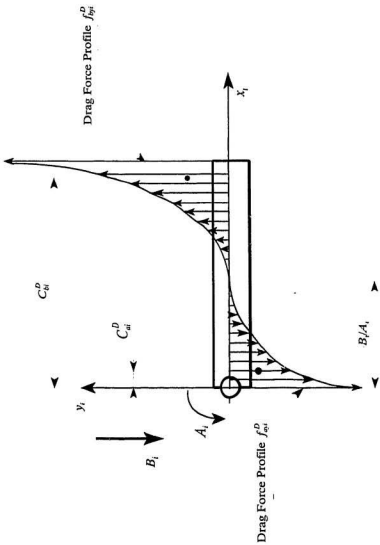


Figure 3-4 Force Profile of Link i of a Planar Revolute Arm (Case II)

Excluding the links preceding we can find an expression for the total torque on joint j caused by the y , drag component of the forces acting on the links following link j :

$$\tau_j^{Dy} = \sum_{i=j}^n \tau_{i,j}^{Dy} \quad 3-1-23$$

Taking into account equations 3-1-7 and 3-1-8 from dimensional analysis, and equations 3-1-11 and 3-1-12, the drag coefficients can be described by either of the following functional equations:

$$\left. \begin{aligned} C_{Dyi} &= \phi \left(\frac{A_i L_i^2}{v}, \frac{A_i L_i}{B_i}, \frac{L_i}{D_i} \right) \\ C_{Dyi} &= \phi \left(\frac{B_i D_i}{v}, \frac{A_i L_i}{B_i}, \frac{L_i}{D_i} \right) \end{aligned} \right\} \quad 3-1-24$$

For case I (figure 3-4) C_m and C_h can be obtained from :

$$\left. \begin{aligned} C_{at}^D &= \frac{\int_0^{l_i} (A_i x_i + B_i)^2 x_i dx_i}{\int_0^{l_i} (A_i x_i + B_i)^2 dx_i} = \frac{L_i}{4} \left[\frac{3A_i^2 L_i^2 + 6B_i^2 + 8B_i A_i L_i}{A_i^2 L_i^2 + 3B_i^2 + 3B_i A_i L_i} \right] \\ C_{ht}^D &= 0 \end{aligned} \right\} \quad 3-1-25$$

For case II (figure 3-5):

$$\left. \begin{aligned}
 C_{ai}^D &= \frac{\frac{B_i}{A_i} \int_0^{\frac{B_i}{A_i}} (A_i x_i + B_i)^2 x_i dx_i}{\frac{B_i}{A_i} \int_0^{\frac{B_i}{A_i}} (A_i x_i + B_i)^2 dx_i} = -\frac{1}{4} \frac{B_i}{A_i} \\
 C_{bi}^D &= \frac{\frac{B_i}{A_i} \int_{\frac{B_i}{A_i}}^{L_i} (A_i x_i + B_i)^2 x_i dx_i}{\frac{B_i}{A_i} \int_{\frac{B_i}{A_i}}^{L_i} (A_i x_i + B_i)^2 dx_i} = \frac{1}{4} \frac{3A_i L_i - B_i}{A_i}
 \end{aligned} \right\} \quad 3-1-26$$

In a similar way we can determine the drag x_i component of the hydrodynamic force acting on link i :

$$f_{xi}^D = C_{Dhi} \frac{\pi}{8} \rho D_i^2 \operatorname{sgn}(u_{xi}) u_{xi}^2 \quad 3-1-27$$

The torque on joint j caused by the drag x_i component of the hydrodynamic force on link i by u_{xi} can be determined from the following expression:

$$\tau_{i,j}^{Dx} = f_{xi}^D \left[\sum_{q=j}^{i-1} L_q \sin \left(\sum_{p=q+1}^i \theta_p \right) \right] \quad 3-1-28$$

Excluding the links preceding, we can find an expression for the total torque on joint j

caused by the x , drag component of the forces acting on the links following link j :

$$\tau_j^{Dx} = \sum_{i=j}^n \tau_{i,j}^{Dx} \quad 3-1-29$$

The total torque on joint j caused by the drag force on the following links, including link j can be determined from the summation:

$$\tau_j^D = \tau_j^{Dy} + \tau_j^{Dx} \quad 3-1-30$$

The inertia component of Morison's equation, in the y_i and x_i directions, can be calculated in a way similar to the drag component. This inertia component will be zero in the case of a single link undergoing either constant rotation or constant translation. However the simple combination of constant rotation and constant translation will result in acceleration. For the general case of accelerated motion, $\ddot{\theta}_j \neq 0$ and $u_0 \neq 0$, the acceleration distribution function along the link i is of the type $f(x_i) = M_i x_i + N_i$, where:

$$N_i = \left. \begin{aligned} & \left[\sum_{j=1}^{i-1} \ddot{\theta}_j \left(\sum_{q=j}^{i-1} L_q \cos \left(\sum_{p=j+1}^i \theta_p \right) \right) \right. \\ & \left. - \sum_{j=1}^{i-1} \ddot{\theta}_j \left(\sum_{q=j}^{i-1} L_q \left(\sum_{p=q+1}^i \ddot{\theta}_p \sin \left(\sum_{p=j+1}^i \theta_p \right) \right) \right) \right] \\ & + \left[u_0 \cos \left(\sum_{j=1}^i \theta_j \right) - u_0 \sum_{j=1}^i \ddot{\theta}_j \sin \left(\sum_{j=1}^i \theta_j \right) \right] \end{aligned} \right\} \quad 3-1-31$$

$$M_i = \sum_{j=1}^i \ddot{\theta}_j \quad 3-1-32$$

In the case where $-N_i/M_i \leq 0$ and $-N_i/M_i > L_i$, it is sufficient to have one interval for the integration from 0 to L_i . If $0 < -N_i/M_i < L_i$, then there are two integration intervals. The integration intervals are from 0 to $-N_i/M_i$ and from $-N_i/M_i$ to L_i . If $-N_i/M_i \leq 0$ and $-N_i/M_i > L_i$ (case I) then:

$$\left. \begin{aligned} f_{ayi}^I &= C_{Myi} \rho \frac{\pi D_i^2}{4} \operatorname{sgn}(\dot{u}_{yi}(L_i)) \int_0^{L_i} (M_i x_i + N_i) dx_i \\ &= C_{Myi} \rho \frac{\pi D_i^2}{4} \operatorname{sgn}(\dot{u}_{yi}(L_i)) \left(N_i L_i + \frac{M_i L_i^2}{2} \right) \\ f_{byi}^I &= 0 \end{aligned} \right\} \quad 3-1-33$$

If $-N_i/M_i > 0$ and $-N_i/M_i < L_i$ (case II) then:

$$\left. \begin{aligned} f_{ayi}^I &= C_{Myi} \rho \frac{\pi}{4} D_i^2 \operatorname{sgn}(-\dot{u}_{yi}(L_i)) \int_0^{-\frac{N_i}{M_i}} (M_i x_i + N_i) dx_i \\ &= C_{Myi} \rho \frac{\pi}{4} D_i^2 \operatorname{sgn}(-\dot{u}_{yi}(L_i)) \left(-\frac{N_i^2}{2M_i} \right) \\ f_{byi}^I &= C_{Myi} \rho \frac{\pi}{4} D_i^2 \operatorname{sgn}(\dot{u}_{yi}(L_i)) \int_{-\frac{N_i}{M_i}}^{L_i} (M_i x_i + N_i) dx_i \\ &= C_{Myi} \rho \frac{\pi}{4} D_i^2 \operatorname{sgn}(\dot{u}_{yi}(L_i)) \left(N_i L_i + \frac{M_i L_i^2}{2} + \frac{N_i^2}{2M_i} \right) \end{aligned} \right\} \quad 3-1-34$$

The torque on joint j caused by the y , inertia component of the hydrodynamic force on

link i by \ddot{u}_y , can be determined from the following expression:

$$\tau_{i,j}^{Iy} = \left[C_{ai}^I + \sum_{q=j}^{i-1} L_q \cos \left(\sum_{p=q+1}^i \theta_p \right) \right] f_{ayi}^I + \left[C_{bi}^I + \sum_{q=j}^{i-1} L_q \cos \left(\sum_{p=q+1}^i \theta_p \right) \right] f_{byi}^I \quad 3-1-35$$

Excluding the links preceding j we can find an expression for the total torque on joint j caused by the y , inertia component of the forces acting on the links following link j :

$$\tau_j^{Iy} = \sum_{i=j}^n \tau_{i,j}^{Iy} \quad 3-1-36$$

The inertia coefficients can be described by either of the following functional equations:

$$\left. \begin{aligned} C_{Myi} &= \phi \left(\frac{A_i L_i^2}{v}, \frac{A_i L_i}{B_i}, \frac{L_i}{D_i} \right) \\ C_{Myi} &= \phi \left(\frac{B_i D_i}{v}, \frac{A_i L_i}{B_i}, \frac{L_i}{D_i} \right) \end{aligned} \right\} \quad 3-1-37$$

For case I C_{ai} and C_{bi} can be obtained from:

$$\left. \begin{aligned} C_{ai}^I &= \frac{\int_0^{l_i} (M_i x_i + N_i) x_i dx_i}{\int_0^{l_i} (M_i x_i + N_i) dx_i} = \frac{L_i}{3} \left[\frac{3N_i + 2M_i L_i}{2N_i + M_i L_i} \right] \\ C_{bi}^I &= 0 \end{aligned} \right\} \quad 3-1-38$$

For case II:

$$\left. \begin{aligned}
 C_{ai}^I &= \frac{\frac{L_i}{M_i} \int_0^{L_i} (M_i x_i + N_i) x_i dx_i}{\frac{N_i}{M_i} \int_0^{L_i} (M_i x_i + N_i) dx_i} = -\frac{1}{3} \frac{N_i}{M_i} \\
 C_{bi}^I &= \frac{\frac{N_i}{M_i} \int_0^{L_i} (M_i x_i + N_i) x_i dx_i}{L_i \int_0^{L_i} (M_i x_i + N_i) dx_i} = \frac{2M_i L_i - N_i}{3M_i}
 \end{aligned} \right\} \quad 3-1-39$$

The inertia component of the force in the x_i direction is equal to:

$$f_{axi}^I = C_{Mxi} \rho \frac{\pi D_i^2}{4} L_i \dot{u}_{xi} \quad 3-1-40$$

The torque on joint j caused by the inertia x_i component of the hydrodynamic force on link i due to \dot{u}_{xi} , can be determined from the following expression:

$$\tau_{i,j}^{Ix} = f_{xi}^I \left[\sum_{q=j}^{i-1} L_q \sin \left(\sum_{p=q+1}^i \theta_p \right) \right] \quad 3-1-41$$

The total torque on joint j caused by the inertia force on the following links,

excluding link j can be determined from:

$$\tau_j^{Ix} = \sum_{i=j}^n \tau_{i,j}^{Ix} \quad 3-1-42$$

The total torque on joint j caused by the inertia force on the following links, including link j can be determined from the summation:

$$\tau_j^I = \tau_j^{Iy} + \tau_j^{Ix} \quad 3-1-43$$

Then the total torque caused by the hydrodynamics forces on link j is equal to:

$$\tau_j^H = \tau_j^I + \tau_j^D \quad 3-1-44$$

In the case of our model it is important to consider the effects of the relative position of the two links, the parallel distance and the planar angle between the two links, on the drag and inertia coefficients. These factors will be included in the neural network identification routine described in chapter 5.

3.2 Mechanical Losses

Friction is often neglected because it is difficult to model and poorly understood. In robotic manipulators friction can account for as much as one third of the applied torque. This is not the case of a manipulator moving underwater, where the hydrodynamic forces usually dwarf the frictional and dynamic forces. Nevertheless friction is not negligible because underwater robot arms often have special sealing systems able to cope

with high pressures, and these increase friction at the joints (Yoerger et al., 1991). The static-kinetic friction transition near zero velocity causes stick-slip behaviour that limits the fidelity of position and control. In addition the load and velocity dependence of friction degrades the tracking ability of simple controllers.

The purpose of including a brief account of mechanical losses in this work is to try to isolate the hydrodynamic forces. Rather than come up with a new model, the treatment of friction here will be patterned after Dupont, 1993 and Dhanaraj, 1990.

Our model was designed bearing in mind the need to isolate the hydrodynamic forces, and although this is not entirely possible, steps were taken in order to minimize the effect of friction and other dissipating phenomena. In fact calibration shows that the overall dissipating torques, including dynamic torques, are insignificant but not negligible in comparison with the overall torque (less than 2% of the measured torque). The calibration was conducted on the physical model by measuring the torques at the joints while unloaded and out of the water.

The unloaded frictional torque for a lubricated ball bearing appears to follow the Petroff law (Dimarogonas, 1989):

$$\tau_o^f = f_o d^3 (\mu n)^{\frac{2}{3}} \quad 3-2-1$$

In the above expression f_o is a function of the type of bearing found in most manufacturers' catalogues, d is the pitch diameter of the bearing, μ is the dynamic viscosity of the lubricant and n is the speed of rotation in RPM. A loaded bearing,

however, seems to follow the Coulomb law:

$$\tau_l^f = f_l W d \left(\frac{W}{C_o} \right)^c \quad 3-2-2$$

where f_l and c depend upon the type of bearing, W is the applied equivalent radial load, and C_o is the static load capacity of the bearing. Notice that the units in the above expressions should be consistent. Rough estimates of coefficients of friction can be found in manufacturers catalogues.

The friction of a lip oil seal is much more difficult to model. It is non-linear and depends on many parameters (Czernik and Horve 1993). A good approximation of this frictional torque can be obtained from:

$$\tau_s^f = 10^{-3} 2\pi R_s^3 R_L f_s \quad 3-2-3$$

where f_s is the coefficient of friction between the material of the seal and the material of the shaft (for a shaft of polished steel $f_s \approx 0.5$), R_L is the interference load between the shaft and the seal ($R_L \approx 0.08$ for recommended values of tolerances) and R_s is the radius of the shaft.

Thus, the total torque at a given joint due to frictional effects is equal to:

$$\tau^f = \tau_o^f + \tau_l^f + \tau_s^f \quad 3-2-4$$

It should be noted that the direction of the frictional torque is always opposite to the

rotation of the joint, a signum function added to the expression accounts for it. The above equations are empirical, and while it is possible to identify the dominant sources of friction in a given system, the actual parameter values should be identified by experiments, since the above expressions do not provide exact results. Because of the complexity of friction models in individual components, robotic researchers typically consider an aggregate friction model for each joint of the robotic arm (Dupont, 1993). The calibration of the dissipating torques has been included in the identification routine. The dissipation of energy in the gear train and in the timing belt transmission were also considered following the manufacturer's recommendations.

3.3 The dynamic equations of motion

The equations of motion of the manipulator are a description of the relationship between the input joint torques and the motion of the arm linkage. The inverse dynamics problem is solved to calculate the input torques necessary to obtain a desired output. The forward dynamics problem solution, the calculation of the motion given the input torques, is mainly used in simulations. The above mentioned process yields the closed-form dynamic equations of motion which can be derived through different methods abounding in the literature.

In the scope of this thesis, however, efficient algorithms for the solution of the inverse dynamics problem will not be discussed; we will be almost entirely relying on Asada and Slotine (1986) and Schilling (1990) for the derivation of the equations of motion. The choice of this thesis is the Lagrangian formulation, which describes the

behaviour of the dynamic system in terms energy, instead of dealing with forces and moments of individual members as the Newton-Euler formulation does. The Lagrangian approach has the advantage that each of the terms in the final closed-form equation has a simple physical interpretation in terms of such things as manipulator inertia, gravity, friction, hydrodynamic, and Coriolis and centrifugal forces. The Lagrangian can be written as:

$$\mathcal{L}(q_i, \dot{q}_i) = T - U \quad 3-3-1$$

where T is the total kinetic energy and U is the potential energy stored in the dynamic system. The equations of motion are given by:

$$\frac{d}{dt} \frac{\partial \mathcal{L}}{\partial \dot{q}_i} - \frac{\partial \mathcal{L}}{\partial q_i} = Q_i \quad 3-3-2$$

Here Q_i is the generalized load corresponding to the generalized coordinate q_i . The generalized loads are residual loads acting on the arm once the loads associated with kinetic and potential energy are removed. In our case, the friction and hydrodynamic loads are generalized loads.

The kinetic energy of a link i in a planar revolute manipulator (figure 3-2) has the form:

$$T_i = \frac{1}{2} m_i u_{ci}^T u_{ci} + \frac{1}{2} \omega_i^T I_i \omega_i \quad 3-3-3$$

Then the total kinetic energy of the linkage is:

$$T = \frac{1}{2} \sum_{i=1}^n (m_i \dot{q}^T J_L^{(i)T} J_L^{(i)} \dot{q} + \dot{q}^T J_A^{(i)T} I_i J_A^{(i)} \dot{q}) = \frac{1}{2} \dot{q}^T H \dot{q} \quad 3-3-4$$

In the above expression m_i is the mass of the link i , I_i is the inertia tensor at the centroid of the link, expressed in the base coordinates, u_{ci} is the velocity vector of the centroid of the link i , ω_i is the angular vector with reference to the base coordinate and J_L and J_A are the Jacobian matrices for linear and angular velocities respectively.

For a two link planar revolute joint arm the result is:

$$u_{c1} = \begin{bmatrix} 0 & -L_{c1} \sin \theta_1 & 0 \\ 1 & L_{c1} \cos \theta_1 & 0 \end{bmatrix} \begin{bmatrix} u_0 \\ \dot{\theta}_1 \\ \dot{\theta}_2 \end{bmatrix} \quad 3-3-5$$

$$u_{c2} = \begin{bmatrix} 0 & -L_1 \sin \theta_1 - L_{c2} \sin(\theta_1 + \theta_2) & -L_{c2} \sin(\theta_1 + \theta_2) \\ 1 & L_1 \cos \theta_1 + L_{c2} \cos(\theta_1 + \theta_2) & L_{c2} \cos(\theta_1 + \theta_2) \end{bmatrix} \begin{bmatrix} u_0 \\ \dot{\theta}_1 \\ \dot{\theta}_2 \end{bmatrix} \quad 3-3-6$$

Using the rotation matrix we determine the inertia tensor of link 1 (a hollow cylinder) and for link 2 (a solid cylinder) in the base coordinates (figure 5-3):

$$I_1 = \frac{m_1}{48} (3D_1^2 + d_1^2 + 4L_1^2) \begin{bmatrix} \sin^2 \theta_1 & -\sin \theta_1 \cos \theta_1 & 0 \\ -\sin \theta_1 \cos \theta_1 & \cos^2 \theta_1 & 0 \\ 0 & 0 & 1 \end{bmatrix} \quad 3-3-7$$

$$I_2 = \frac{m_2}{48} (3D_2^2 + 4L_2^2) \begin{bmatrix} \sin^2(\theta_1 + \theta_2) & -\sin(\theta_1 + \theta_2)\cos(\theta_1 + \theta_2) & 0 \\ -\sin(\theta_1 + \theta_2)\cos(\theta_1 + \theta_2) & \cos^2(\theta_1 + \theta_2) & 0 \\ 0 & 0 & 1 \end{bmatrix} \quad 3-3-8$$

The manipulator inertia tensor matrix is a matrix based on the individual inertia tensors:

$$H = \sum_{i=1}^n (m_i J_{L_i}^{(i)T} J_{L_i}^{(i)} + J_{A_i}^{(i)T} I_i J_{A_i}^{(i)}) \quad 3-3-9$$

$$\left. \begin{aligned} H_{21} &= m_1 L_{c1} \cos \theta_1 + m_2 (L_1 \cos \theta_1 + L_{c2} \cos(\theta_1 + \theta_2)) \\ H_{22} &= m_1 L_{c1}^2 + I_1 + m_2 (L_1^2 + L_{c2}^2 + 2L_1 L_{c2} \cos \theta_2) + I_2 \\ H_{23} &= m_2 L_1 L_{c2} \cos \theta_2 + m_2 L_{c2}^2 + I_2 \\ H_{31} &= m_2 L_{c2} \cos(\theta_1 + \theta_2) \\ H_{32} &= m_2 L_1 L_{c2} \cos \theta_2 + m_2 L_{c2}^2 + I_2 \\ H_{33} &= m_2 L_{c2}^2 + I_2 \end{aligned} \right\} \quad 3-3-10$$

Now the first term in the Lagrangian formulation can be calculated:

$$\frac{d}{dt} \frac{\partial T}{\partial \dot{\theta}_i} = \frac{d}{dt} \left(\sum_{j=1}^2 H_{ij} \dot{\theta}_j \right) = \sum_{j=1}^2 H_{ij} \ddot{\theta}_j + \sum_{j=1}^2 \frac{dH_{ij}}{dt} \dot{\theta}_j \quad 3-3-11$$

Excluding the gravity forces we obtain an expression for the generalized load at joint i :

$$Q_i = \sum_{j=1}^n H_{ij} \dot{q}_j + \sum_{j=1}^n \sum_{k=1}^n h_{ijk} \dot{q}_j \dot{q}_k \quad 3-3-12$$

where:

$$\left. \begin{aligned} h_{223} &= -2m_2 L_1 L_{c2} \sin(\theta_1 + \theta_2) \\ h_{233} &= -m_2 L_1 L_{c2} \sin \theta_2 \\ h_{322} &= m_2 L_1 L_{c2} \sin \theta_2 \end{aligned} \right\} \quad 3-3-13$$

The first term of equation 3-2-12 represents the inertia torques, including interaction torques, and the second accounts for the Coriolis and centrifugal effects. Notice that the gravity term has not been included since the two link planar model moves in a plane perpendicular to the direction of the gravity and buoyancy forces. However these forces and reaction moments will have to be taken into account while calculating the friction at the joints. The friction, including the efficiency of the transmission, and the hydrodynamic forces will be included in the generalized load Q_i . However because they are difficult to model the friction and transmission effects were experimentally calibrated.

The torques at the joints 1 and 2 due only to dynamic loads are:

$$\begin{aligned}
 \tau_1 &= \left[H_{21}\ddot{u}_0 + H_{22}\ddot{\theta}_1 + H_{23}\ddot{\theta}_2 \right] + \dot{\theta}_1\dot{\theta}_2 h_{223} + \dot{\theta}_2 h_{233} \\
 &= \left[m_1 L_{c1}^2 + \frac{m_1(3D_1^2 + d_1^2 + 4L_1^2)}{48} + m_2(L_1^2 + L_{c2}^2 + 2L_1 L_{c2} \cos \theta_2) \right. \\
 &\quad \left. + \frac{m_2(3D_2^2 + 4L_2^2)}{48} \right] \ddot{\theta}_1 + \left[m_2(L_1 L_{c2} \cos \theta_2 + L_{c2}^2) + \frac{m_2(3D_2^2 + 4L_2^2)}{48} \right] \ddot{\theta}_2 \\
 &\quad + [m_1 L_{c1} \cos \theta_1 + m_2(L_1 \cos \theta_1 + L_{c2} \cos(\theta_1 + \theta_2))] \ddot{u}_0 \\
 &\quad - m_2 L_1 L_{c2} \sin \theta_2 \left(\dot{\theta}_1 \dot{\theta}_2 + \frac{\dot{\theta}_2^2}{2} \right)
 \end{aligned} \quad \left. \vphantom{\tau_1} \right\} 3-3-14$$

$$\begin{aligned}
 \tau_2 &= \left[H_{31}\ddot{u}_0 + H_{32}\ddot{\theta}_1 + H_{33}\ddot{\theta}_2 \right] + \dot{\theta}_2^2 h_{322} \\
 &= \left[m_2(L_1 L_{c2} \cos \theta_2 + L_{c2}^2) + \frac{m_2(3D_2^2 + 4L_2^2)}{48} \right] \ddot{\theta}_1 \\
 &\quad + \left[m_2 L_{c2}^2 + \frac{m_2(3D_2^2 + 4L_2^2)}{48} \right] \ddot{\theta}_2 + [m_2 L_{c2} \cos(\theta_1 + \theta_2)] \ddot{u}_0 \\
 &\quad + (m_2 L_1 L_{c2} \sin \theta_2) \dot{\theta}_2
 \end{aligned} \quad \left. \vphantom{\tau_2} \right\} 3-3-15$$

The manipulator model developed for this work has the second link remotely driven, as shown in figure 4-3, by a timing belt powered at the base. This eliminates the reaction torque at joint 2 and only an insignificant friction torque remains.

Therefore the virtual dynamic torques exerted at the joints τ_1 and τ_2 are:

$$\delta Work = \tau_1 \delta \theta_1 + \tau_2 (\delta \theta_1 + \delta \theta_2) = (\tau_1 + \tau_2) \delta \theta_1 + \tau_2 \delta \theta_2$$

$$\tau_1 + \tau_2 = \tau_1^* \quad \tau_2^* = \tau_2 \quad 3-3-16$$

A program for the computation of the joint torques based on the mathematical model is listed in Appendix D.2. Output from the model will be compared with experimental data in Chapter 5.

Chapter 4

Wave Tank Experiment

4.1 Design of the Two-Link Planar Revolute Arm Model

The experimental model designed to measure joint torques was a two-link planar, fully revolute arm. The model itself has two degrees of freedom, moving only in the horizontal plane. It was mounted on the towing carrier in the wave tank facility at the Memorial University of Newfoundland.

A picture of the setup out of the water is presented in figure 4-1. The two links are independently driven, the second link is driven from the base (see equation 3-3-16). The first link, figure 4-3, is hollow and is driven by a DC motor, a gear train with a reduction rate of 25 and a vertical hollow shaft, figure 4-2. A torque sensor has been mounted between the DC motor and the gear train, coupled with compensating couplings as recommended by the sensor's manufacturer in order to eliminate radial and axial loads. The gear train and the vertical hollow shaft are mounted on high precision self-aligning bearings. This compensates for manufacturing errors and minimizes friction. The gears

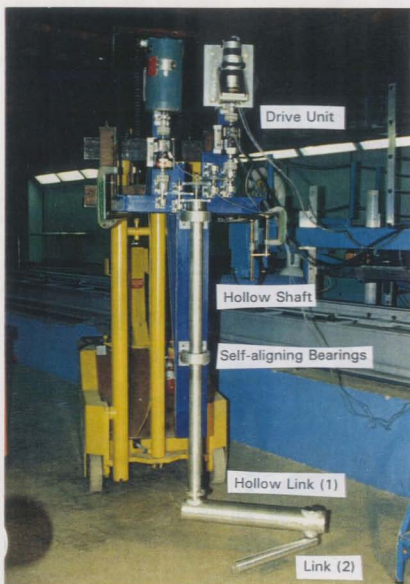


Figure 4-1 Experimental Setup of a Two-Link Underwater Arm Model

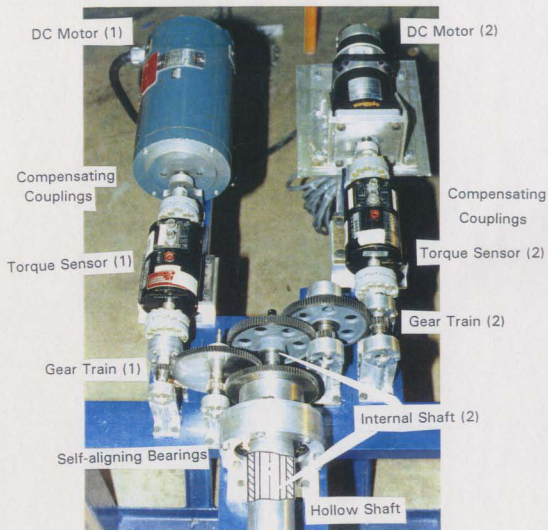


Figure 4-2 Detail of the Driving Section of the Setup

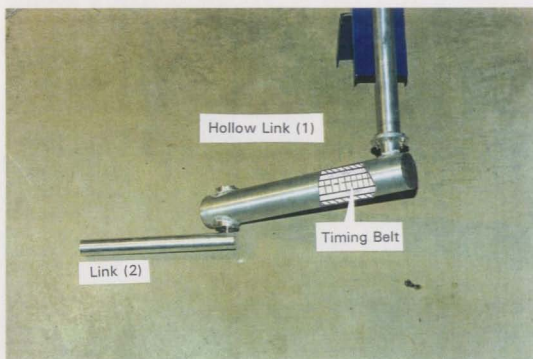


Figure 4-3 Two-Link Underwater Arm Model

are also high precision and with minimal backlash characteristics. This enables us to measure reverse loads accurately and to minimize friction as well.

The second link is driven from the base by a second DC motor, a gear train of the same characteristics as the first and a shaft mounted on self-aligning bearings inside the hollow shaft attached to the first link. A timing pulley is mounted at the end of the shaft and through a timing belt drives a second pulley mounted at the end of the hollow link, figure 4-3. A double-lip oil seal was installed between the two links, fortunately the friction due to the seal does not depend on the radial load applied, and does not vary significantly with the relative circular speed between the shaft and the seal.

In order to measure the position of the links, potentiometers were installed in the shafts of the gear trains.

4.2 Testing

It is impossible to test every possible combination of configuration and velocities since the number is too great.

The first stage of the experiment included towing the model at speeds ranging from 0.3 to 1.25 m/sec while the joints were fixed at specific angular positions (figure 3-2). For example for the angular position of joint 1 $\theta_1=0$, the angular position of joint 2 was also set to $\theta_2=0$, the model was then towed at 0.3 m/sec. This constitutes one data file. For the same angular positions the model was towed at different speeds from 0.3 m/sec to 1.25 m/sec. The same procedure was repeated for different values of θ_1 and θ_2 , spaced by 15 degrees. The upper limit of 1.25 m/sec was set to avoid high stresses and vibrations on the mechanism. The lower limit of 0.3 m/sec is due to the fact that the

torque sensors **did not** shed accurate readings **below this** limit. Most manipulators of AUVs/ROVs **work well** within the specified limits.

The **second** stage consisted of steady rotations and zero towing velocity. First, joint 1 was **locked in** position while joint 2 was rotated at different angular velocities up to 34 RPMs **approximately**. A data file consists of data collected at a specific angular velocity. **Secondly**, joint 2 was locked in place while rotating joint 1. At this point it must be noted **that** link 2 was driven from the base and joint 2 was locked relative to the base **not to the first** link. This means that in order to virtually lock the second link relative to the first, the **second** joint had to be rotated from the base at the same angular velocity as the first one. Finally, both joints were rotated at different angular velocities.

The **third** stage included steady translations (constant towing velocity) and rotations of both links. **The** testing basically consisted of a superposition of the first and the second stage, needless to say that the possible number of combinations is elevated. Since the towing mechanism and the DC motors controls were operated manually by two persons the total number of data files collected was limited. A total of 527 data files were collected.

4.3 Data Acquisition and Processing

Most experimental setups can be considered as systems, with input signals providing excitation, and output signals corresponding to some property of the system. In our case, for instance, a model of a two-link planar revolute robot arm under the influence of the fluid in which it moves (input) would have as output signals torques at the joints caused by the drag force acting on the links, and the angular position of the two joints.

Signals in the real world are continuous or analog, meaning they are dependent on time even if theoretically they are not: noise in the system affects the magnitude of the signal. The amount of processing which can be done on analog signals is severely limited, basically only addition and multiplication without special hardware. By converting analog signals to digital form, a wide range of analysis becomes possible. However this conversion has many factors which influence the subsequent analysis and should be considered.

The signal that we would normally obtain from an excited transducer is analog in most of the cases. In our case we received two analog signals from the two Rotary Transformer Torque Sensors, and two analog signals from the potentiometers. Usually these analog signals need some processing before converting them to digital form.

The most common type of analog signal processing encountered is amplification and filtering. Amplification is simply the multiplication of a signal by some constant amount in order to boost the signal that may be small. All signals are affected by random noise from circuit devices and systematic noise from fixed sources like AC power lines. Systematic noise could be eliminated by carefully arranging the experimental set up, but random noise can never really be eliminated, only reduced in significance.

Conditioning a signal usually means comparing two signals from a similar source and amplifying the difference in those signals. Since the random noise is present in both signals, the effect of random noise is greatly reduced, as it is basically subtracted from itself, leaving only the signal. The other way to reduce noise in a signal is through filtering. This is best described in the frequency domain, where a filter is basically a

window which lets certain frequencies through and blocks others. The most common type of filter is the low pass filter which lets all frequencies below a certain frequency pass through. In this manner, the effect of higher frequency random noise and systematic noise is reduced.

A/D conversion is usually performed by a computer with a special A/D hardware. The computer could be a PC, a Workstation or a VAX, or it could be the build-in microprocessor of an oscilloscope. A/D converters are rated by two primary features, resolution and speed. The resolution of an A/D converter refers to how many discrete steps it can divide its input into. The more steps the higher the resolution. This number of steps is usually a power of two, since the A/D interacts with a digital computer. Some manufacturers refer to the number of steps when specifying their A/D converters, but it is more common to refer to the power of two. A converter with 256 steps is referred to as an 8 bit converter. Common A/D converters used in experiments are 10, 12, or 16 bit. The input range is one of the important characteristics of A/D converters. This refers to the range of input voltages allowed. For example, a 16 bit converter with a +/- 10 volt range is able to discriminate a 0.3 mV change in input; on the other hand a 16 bit converter with +/- 1 volt input can discriminate a 30 micro volt change. The ability to measure a smaller change in voltage is referred to as higher sensitivity. Another important parameter of an A/D converters is its speed, or rate of conversion, usually measured in conversions per second (hertz). A good converter would have a conversion rate of approximately 50 Hz. This rate is usually higher than typically required for an experiment. Most manufacturers of data acquisition hardware, like National Instruments,

for instance, provide software for the design of the data acquisition setup and also for the data processing.

The tests conducted here sampled data at a rate of 20 Hz with a Keithley 500 A/D converter. The output data file registered values of the joint torques in N.m , considering the reduction rate of the gear train, the angular position of the two joints and the carrier's velocity. The angular velocities were computed by filtering the angular position arrays, for smoothing, with the Signal Processing Toolbox from MATLAB, and then differentiating the resulting arrays in time. A second differentiation produced the joint accelerations. In summary, the raw data file contained the following parameters:

T_1 - Torque at joint 1	[N.m]
T_2 - Torque at joint 2	[N.m]
θ_1 - Angular position of joint 1	[degrees]
θ_2 - Angular position of joint 2	[degrees]
u_c - Velocity of the carrier	[m/sec]

The file processed with MATLAB contained the following parameters:

T_1 - Torque at joint 1	[N.m]
T_2 - Torque at joint 2	[N.m]
θ_1 - Angular position of joint 1 (filtered)	[radians]
θ_2 - Angular position of joint 2 (filtered)	[radians]
u_c - Velocity of the carrier (filtered)	[m/sec]
$\dot{\theta}_1$ - Angular velocity of joint 1	[rad/sec]
$\dot{\theta}_2$ - Angular velocity of joint 2	[rad/sec]

The resulting file from MATLAB was processed with the program listed in appendix B.2 in order to obtain the parameters listed in the table of appendix C. This program contains the mathematical model described in chapter 3 and prepared the data file used to train and test the Neural Network.

4.4 Neural Network System Identification

The procedure used to design, train and test the neural nets used in the scope of this work is outlined in Appendix A. The method used to train the network is backpropagation with supervised learning. This means that the program training the net compares the output from the net with reliable test results: it then generates an error which is used to adjust the weights in the net. A significant number of cycles were required to train the nets used here. The main objective was to train a neural network so it would perform accurately enough when presented with new data.

For the two-link configuration shown in figure 3-2, the net would look something like the one shown in figure 4-4.

The objective was to train a neural net of the type represented in figure 4-4, to compute the joint torques in the two link arm of figure 4-1, when presented with kinematic and dynamic data. Two different input layers were tried. In the first one the following input data were presented:

u_c	Velocity of the carrier	[m/s]
θ_1, θ_2	Joint angles	[radians]
$c\theta_1, c\theta_2$	Cosinus of the joint angles	
$\dot{\theta}_1, \dot{\theta}_2$	Joint angular velocities	[radians/s]

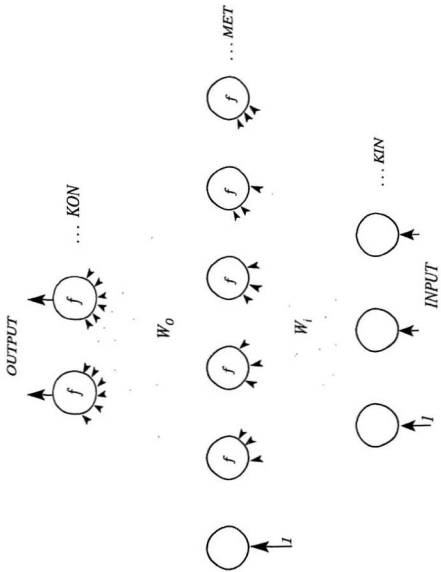


Figure 4-4 Neural Net with common middle layer.

The second input layer of the neural network trained included the following data:

τ_1, τ_2	Joint torques computed following the procedure outlined in chapter 3. but with drag and inertia coefficients equal to 1.
Re_1, Re_2	Reynolds numbers for links 1 and 2
Ret_1, Ret_2	Rotational Reynolds numbers for links 1 and 2
KC_1, KC_2	Variation of the Keulegan-Carpenter numbers
θ_1, θ_2	Joint angles

In both cases the joint torques obtained experimentally, T_1 and T_2 , were the target output to be matched by both neural networks. The parameters included in the second neural network were defined by dimensional analysis and by the application of Morison's equation to this case. In the second case the mathematical model described in chapter 3 was "forced" into the network: something similar to what was done by Zomaya and Nabhan (1993) for the decentralized neuro-adaptive controller for robot motion. As a point of interest we note that the second neural net required less training iterations than the first one: once trained both networks exhibited similar performance. Notice that the dimensions of the links and the physical properties of the fluid have not been included since they were the same for all the samples taken. Both neural nets were trained with 150 sets of data and 8,000 iterations, using the steepest descent method, yielding acceptable results. However as it can be appreciated from the mathematical model described in chapter 3, the torques at joints 1 and 2 depend on the same parameters but in different measure. This is probably why when sufficiently trained the net gives accurate results for the torque at one joint but not the other. It was then decided to try a neural net with

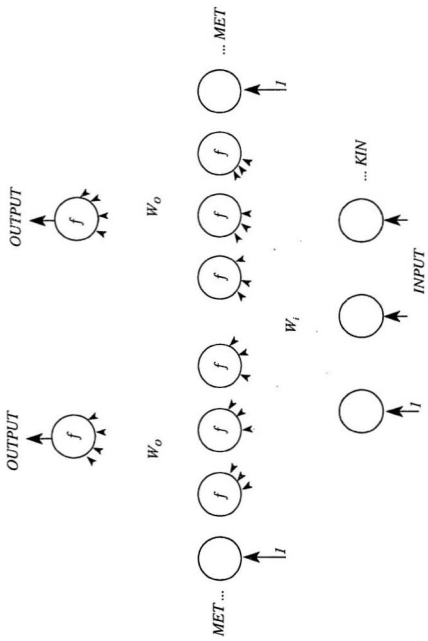


Figure 4-5 Neural Net with parallel middle layers.

parallel middle layers and common input and output layers, figure 4-5. This is the same as having two separate nets, one for each output. Then the error from one output will affect the correction of weights that generate that output but it will have no bearing in the weights that generate the other output. The result was that less neurons in each middle layer could be used, as compared to the common middle layer net, and the results were accurate for both joints. Also fewer cycles were needed to train the net.

The fit of the training data and the performance against new data has been graphically presented in chapter 5 for both types of neural nets. Also, a detailed algorithm and program listing can be found in appendix A and B.

Chapter 5

Experimental and Theoretical Results

A neural network identification program, as described in section 4.4 and appendix A, was trained with selected data sets. The number of data sets included to train the neural net was limited by the simple fact that the time it takes to train a net increases proportionally with the number of data sets. It was necessary to select a sufficient number of data sets that represented most combinations of velocities and angular positions while at the same time keeping that number low in order to keep the training time acceptable. A neural net trained with an insufficient number of data sets, or with data which is not representative of most combinations, will not respond to new data with an acceptable fit. Another key factor is the number of neurons in the middle layer. The robustness of the net is directly proportional to this number, but the time for one training cycle also increases. A number of 24 neurons in the middle layer was determined by trial and error as the minimum number of neurons that responds well to new data.

The data sets used to train the neural net are tabulated in appendix C. The performances of two neural nets were compared: a neural net with a common middle layer and a neural net with two parallel middle layers (figures 4-4 and 4-5 respectively).

Figure 5-1 and 5-2 shows a plot of the torque computed by the net with common middle layer versus the experimental torque for joints 1 and 2 respectively. A straight diagonal line is also plotted to visualize the error, the deviation from a straight line denotes the difference between the test torque and the torque computed by the net. This is the response of the net to the training data itself. The fit would not improve after 8000 training cycles. In figure 5-3 and 5-4 some of the same values are plotted in a different way, the torque computed by the net (a solid line) and the experimental torque (o) are plotted in the same graph versus the time step index. For a sampling frequency of 20 Hz each step corresponds to 0.05 seconds.

Figures 5-5 through 5-10 are similar to the figures described in the previous paragraph but for a neural net with parallel middle layers (section 4.4) . This network has two middle layers with 24 neurons each. Each middle layer connects to only one neuron in the output layer. It can be seen from figures 5-9 and 5-10 that a fit similar to the one represented in figures 5-1 and 5-2 is achieved after only 2000 training cycles. This is due to the fact that the algorithm calculating the adjustment of the weights has to deal with only one error instead of two.

Figures 5-11 through 5-18 show the parameters of a data file selected to contain angular velocities of both links and towing velocity not equal to zero. Figure 5-11 and 5-12 give both the raw and the filtered experimental torques for joints 1 and 2

respectively. The rest of the graphs contain the angular velocities of both joints and the angular positions. The angular position of joint 2 with respect to the base ($\theta_1 + \theta_2$) is also displayed. These data sets were fed into the trained neural net with parallel middle layers. The results are plotted in figures 5-19 through 5-22. The neural net with parallel middle layer performed much better than the net with a common middle layer when presented with the same new data sets. It seems that for this specific problem the parallel scheme is more robust.

The experimental joint torques were compared to those calculated using the mathematical model based on Morison's Equation and the dynamic equations of motion (chapter 3). The results are plotted in figures 5-23 and 5-24. The mathematical model was based on the equations of motion including hydrodynamic forces and friction. It did not include, however, the effect of the two free ends of both links and the near effect of one link on the other. A computer program was developed in order to obtain a numerical output that could be compared to test results. There was an expected discrepancy that could be partially explained by the fact that infinite cylinder data was used in the mathematical model, meaning that three dimensionality effects and the effects of other bodies (the other link) were not accounted for. Although the output from the mathematical model was not far off the test results, there is obviously a need to use a more accurate method for determining the torque at the joints, particularly for applications requiring high precision, i.e. motion control. Finding drag coefficients that account for every possible configuration can be difficult not to mention time consuming since for a multiple link planar arm the drag and inertia coefficient are nested inside each other. The

mechanical losses and the dynamic loads were negligible when compared to the magnitude of the hydrodynamic forces.

The limited data printed in this thesis served the purpose of illustrating the phenomena and the applicability of the neural network to this problem. A companion disk contains the totality of the data collected during the experiments, over 500 files. In case the disk is missing the same can be obtained from the OERC, Faculty of Engineering and Applied Science, Memorial University of Newfoundland. This contains utilities to display the data on the screen and a script file to manipulate the data using MATLAB. A README file explains the procedure to follow and the contents of the disk in detail.

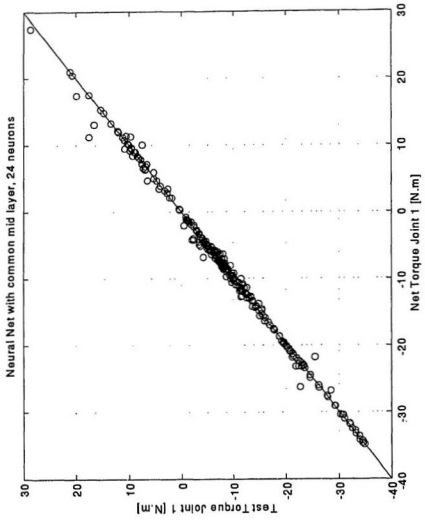


Figure 5-1 Fully trained neural network fit to training data, joint 1 (24 neurons, common middle layers).

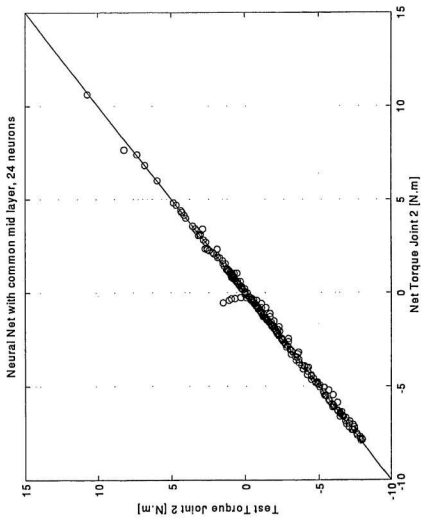


Figure 5-2 Fully trained neural network fit to training data, joint 2 (24 neurons, common middle layers).

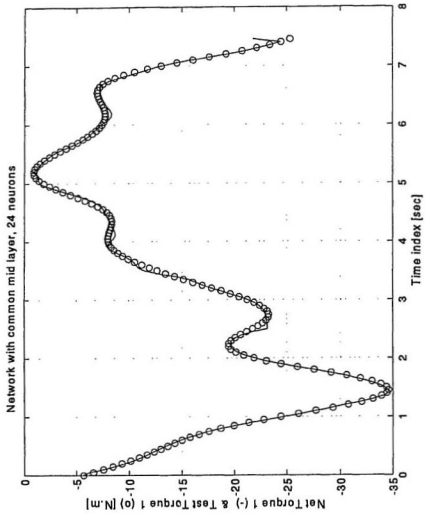


Figure 5-3 Fully trained neural network fit to training data, joint 1 (24 neurons, common middle layers).

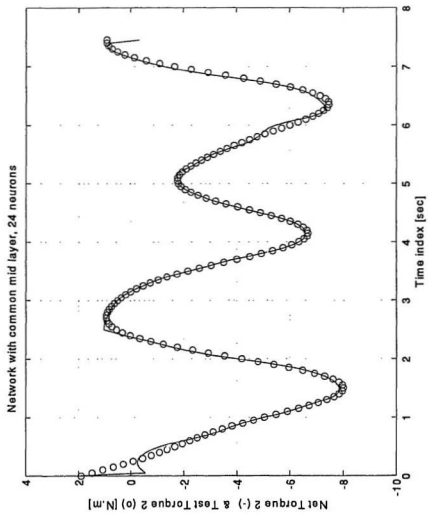


Figure 5-4 Fully trained neural network fit to training data, joint 2 (24 neurons, common middle layers).

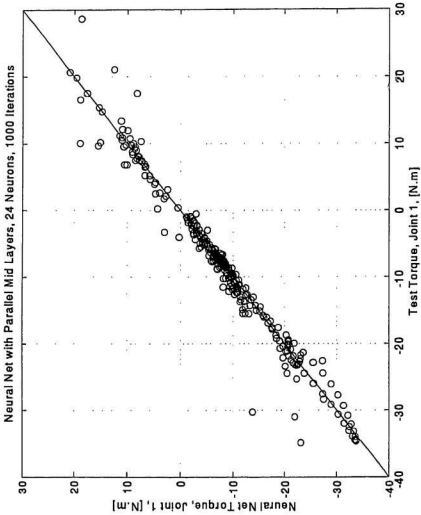


Figure 5-5 1000 cycles trained neural network fit to training data, joint 1 (24 neurons, parallel middle layers).

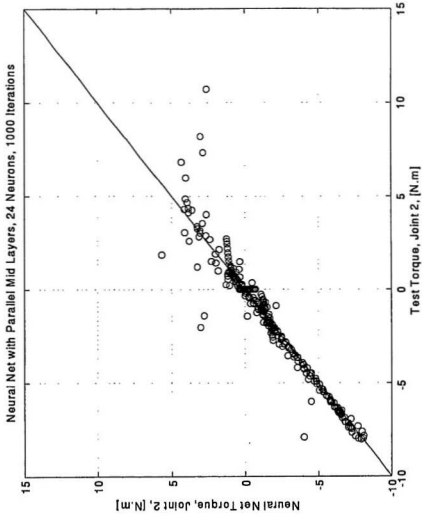


Figure 5-6 1000 cycles trained neural network fit to training data, joint 2 (24 neurons, parallel middle layers).

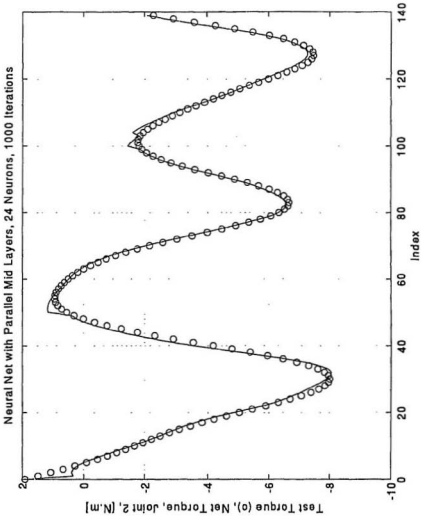


Figure 5-8 1000 cycles trained neural network fit to training data, joint 2 (24 neurons, parallel middle layers).

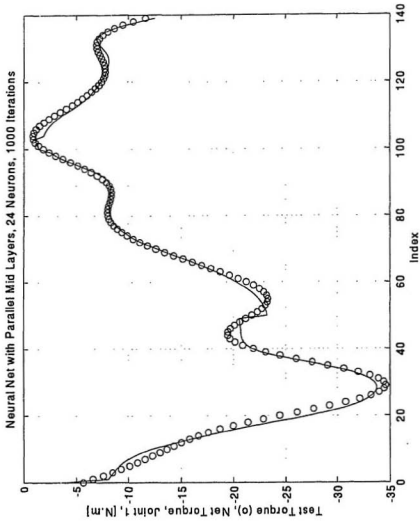


Figure 5-7 1000 cycles trained neural network fit to training data, joint 1 (24 neurons, parallel middle layers).

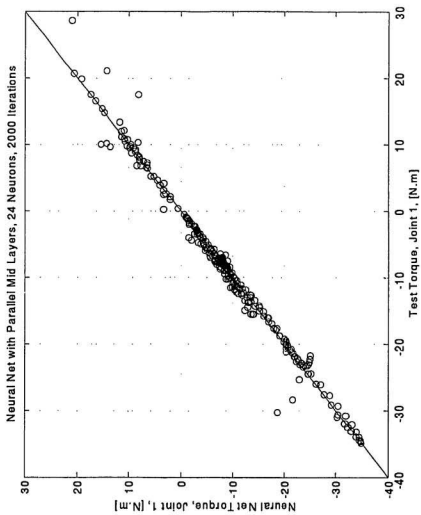


Figure 5-9 2000 cycles trained neural network fit to training data, joint 1 (24 neurons, parallel middle layers).

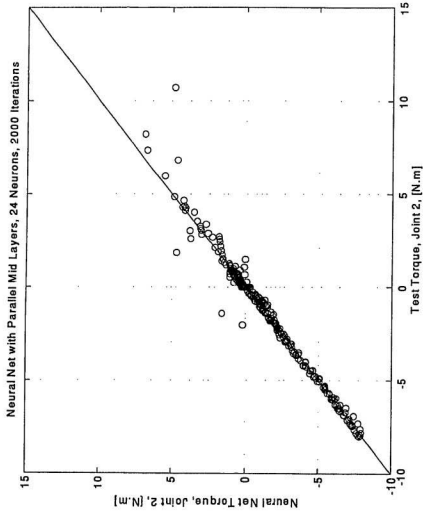


Figure 5-10 2000 cycles trained neural network fit to training data, joint 2 (24 neurons, parallel middle layers).

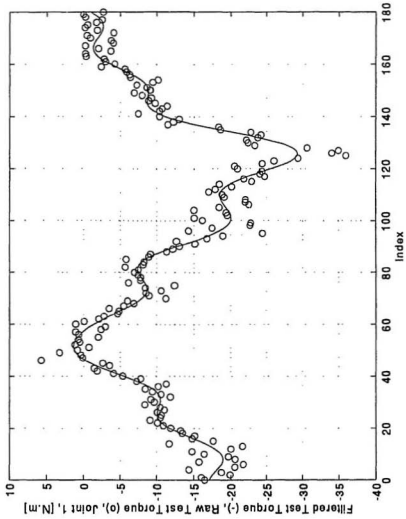


Figure 5-11 New data file presented to the fully trained neural net, raw test torque and filtered test torque vs time index, joint 1.

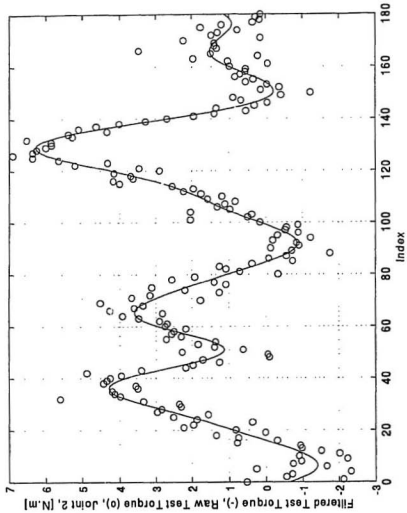


Figure 5-12 New data file presented to the fully trained neural net, raw test torque and filtered test torque vs time index, joint 2.

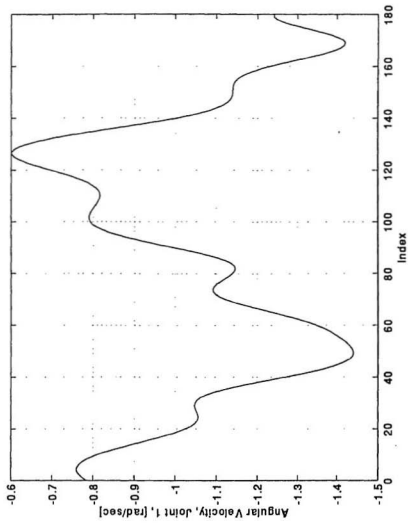


Figure 5-13 New data file presented to the fully trained neural net, angular velocity vs time index, joint 1..

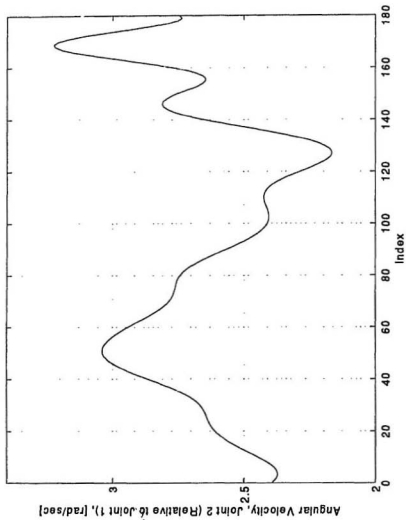


Figure 5-14 New data file presented to the fully trained neural net, angular velocity vs time index, joint 2.. (relative to joint 1).

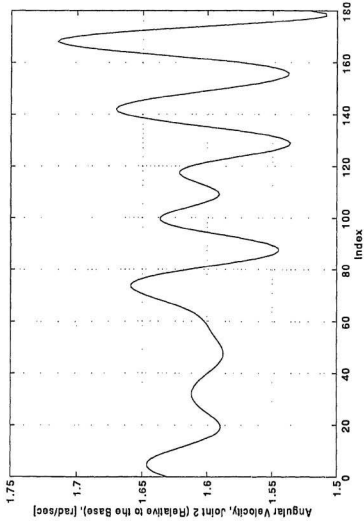


Figure 5-15 New data file presented to the fully trained neural net, angular velocity vs time index, joint 2.. (relative to the base).

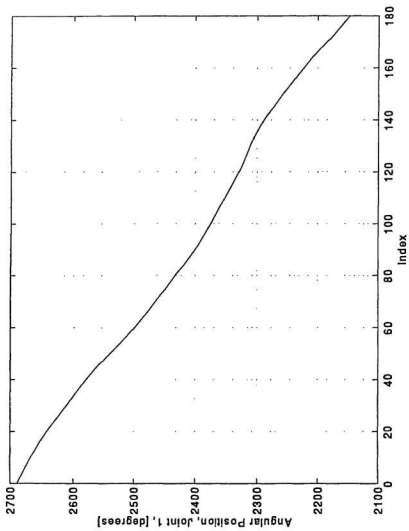


Figure 5-16 New data file presented to the fully trained neural net, angular position vs time index, joint 1..

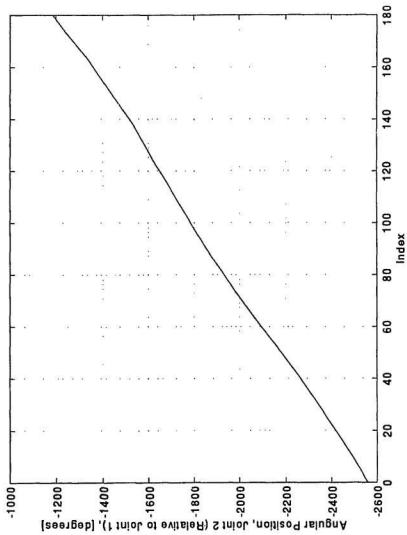


Figure 5-17 New data file presented to the fully trained neural net, angular position vs time index, joint 2.. (relative to joint 1).

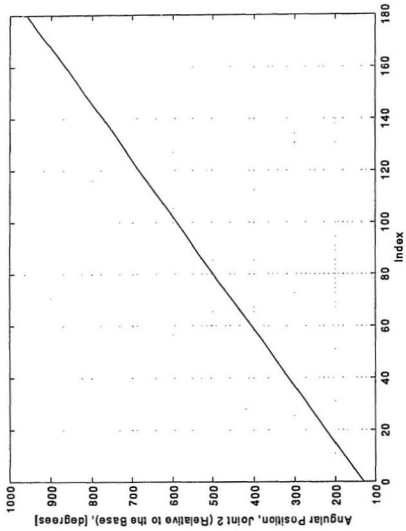


Figure 5-18 New data file presented to the fully trained neural net, angular position vs time index, joint 2.. (relative to the base).

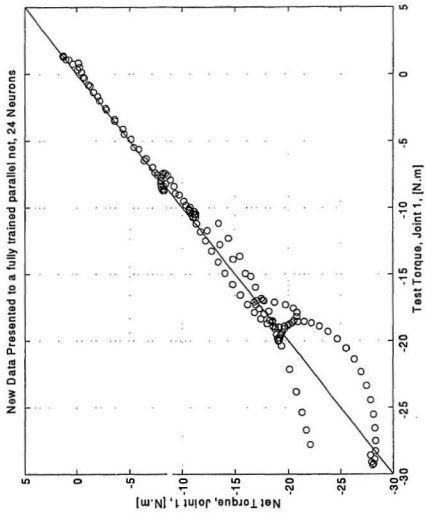


Figure 5-19 Neural network fit to the new data, joint 1 (parallel middle layers)

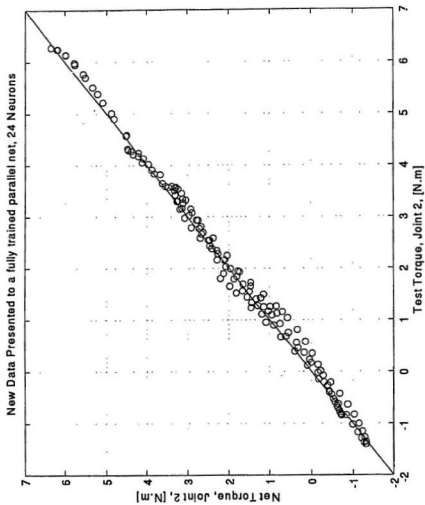


Figure 5-20 Neural network fit to the new data, joint 2 (parallel middle layers)

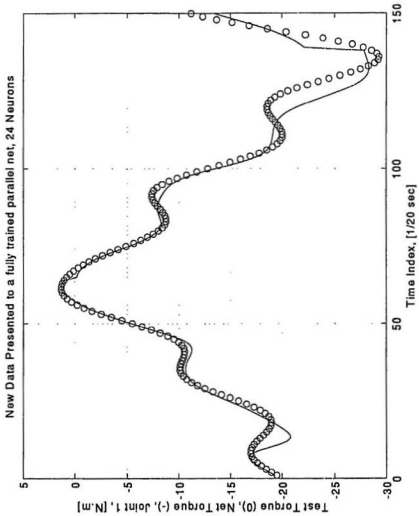


Figure 5-21 Neural network fit to the new data, joint 1 (parallel middle layers)

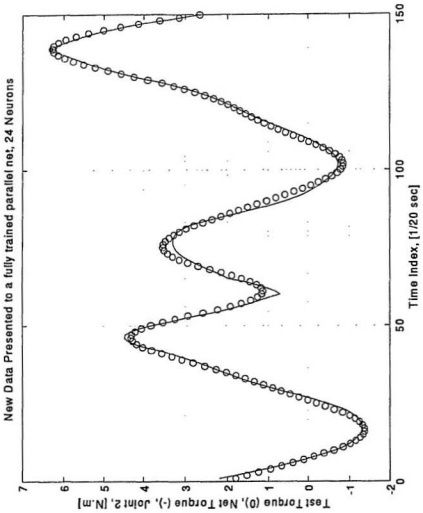


Figure 5-22 Neural network fit to the new data, joint 2 (parallel middle layers)

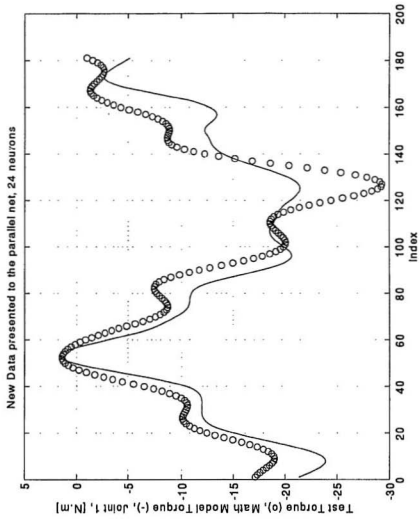


Figure 5-23 Mathematical model fit to new data, joint 1.

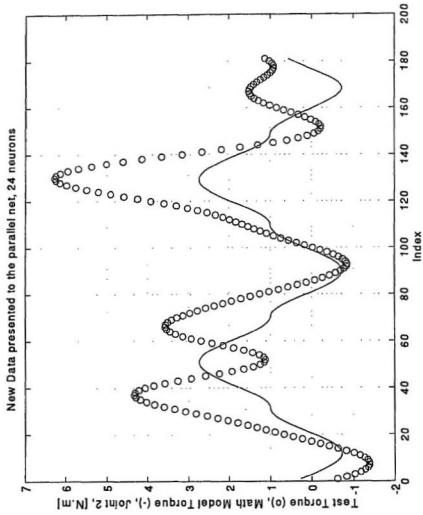


Figure 5-24 Mathematical model fit to new data, joint 2.

Chapter 6

Conclusions

A mathematical model for hydrodynamic loads on a robot arm based on Morison's Equation and dimensional analysis has been developed. The model took into consideration the non-uniform distribution of the hydrodynamic forces along the link through three dimensionless parameters, namely the Reynolds number (Re), the rotational Reynolds number (Ret) and the modified Keulegan-Carpenter number (KC), which were obtained from dimensional analysis. However the drag and inertia coefficients are nested one inside the other, for the case of the two-link model (the torque on link 1 depends on the force on the link 2 and its distribution). This makes it very difficult to present an expression for each drag and inertia coefficient since one drag coefficient would be a function of the other. The drag and inertia coefficients were considered constant for the integration of the force along the link. This was however corrected by making each drag and inertia coefficient a function of the three noted dimensionless parameters. The

hydrodynamic forces were incorporated into the equations of motions using the Lagrangian formulation. An attempt to model friction revealed that for the given experimental model many unknowns remained. The conclusion was that the theoretical model for the mechanical losses was not going to shed accurate results, and therefore it was decided to calibrate them experimentally.

A physical model of a two-link planar revolute joint arm was constructed. Special care was taken to ensure minimal friction and backlash effects, that would have prevented us from taking accurate measurements, particularly during sudden reverse loads. Given the complexity of the data and the number of parameters involved, it was decided to use a neural network identification program. The neural nets trained well and responded adequately to new data. This suggests that it could be used by control designers.

The mathematical model performed poorer than the neural network identification program due to it being based on infinite cylinder data.

Chapter 7

Recommendations

There are few options open as a follow-up of this research. The same experimental model could be used to test the behaviour of the torques, caused by hydrodynamic forces, in response to accelerated motions, or in the presence of waves. A number of links with different L/D ratios could be constructed and tested, and the distance between the axis of the two cylinders, T/D , could also be changed. A more sophisticated controller for the revolutions of the DC motors is strongly recommended. A model of the body of an AUV/ROV could also be placed near the two-link model in order to gain a better understanding of the body-manipulator interaction.

References

- Anaturk, A.R., Tromans, P.S., van Hazendonk, H.C., Sluis, C.M. Otter, A. 1992. "Drag force on cylinders oscillating at small amplitude: A new model.", *Journal of Offshore Mechanics and Arctic Engineering*, Vol. 14, No. 2, May 1992, pp. 91-103.
- Asada, H., Slotine, J.-J.E. 1986. *Robot Analysis and Control*, Wiley-Interscience, 1986.
- Baban, F., Tempe, A.Z., So, R.M.C., Otugen, M.V. 1989. "Unsteady forces on circular cylinders in a cross-flow.", *Experiments in Fluids*, 1989, pp. 293-302.
- Badr, H.M., Dennis, S.C.R., Young, P.J.S. 1989. "Steady and unsteady flow past a rotating circular cylinder at low Reynolds numbers.", *Computers and Fluids*, Vol. 17, No. 4, 1989, pp. 579-609.
- Baker, J.H.A., Sayer, P. 1990. "Selection of Experimental Facility and Measurements of Hydrodynamics Coefficients for ROVs", *First European Offshore Mechanics Symposium, Trondheim, Norway, 20-22 August, 1990*, 12 p.
- Baz, A., Gumusel, L. 1990. "Buoyancy-and Gravity-Powered Underwater Robots", *The International Journal Of Robotics Research*, Vol. 9, no. 5, October 1990, pp. 60-69.
- Berardinis, L. A. 1992. "Clear Thinking on Fuzzy Logic", *Machine Design*, April 1992, pp.46-52.
- Bin, T., Yu-Cheng, L. 1991. "Force coefficients on inclined cylinders in random waves and current.", *Journal of Hydrodynamics*, Vol. 3, No. 3, 1991, pp. 26-34.
- Blevins, R. D. 1990. *Flow Induced Vibration*, Van Nostrand Reinhold, second edition, 1990.
- Blidberg, D., Turner, R. M., Chappell, S. 1991. "Autonomous underwater vehicles. Current activities and research opportunities.", *Robotics and Autonomous Systems*, Vol. 7, No.2-3, August 1991, pp.139-150.
- Burde, G.I. 1990. "Exact solution of the Navier-Stokes equations", *Fluid Dynamics*, Vol. 24, No. 4, January 1990, pp.632-633.
- Caudill, M. 1990. "Neural Networks Primer Part III", *AI Expert*, June 1988, pp. 53-67.
- Chakrabarti, S.K. 1987. *Hydrodynamics of Offshore Structures*, Springer-Verlag Berlin, 1987, 440 p.

- Chew, Y.T., Low, H.T., Wong, S.C., Tan, K.T. 1992. "An unsteady wake-source model for flow past an oscillating circular cylinder and its implications for Morrison's equation", *Journal of Fluid Mechanics*, Vol. 240, 1992, pp.627-650.
- Cox, E. 1993. "Adaptive fuzzy systems", *IEEE spectrum*, February 1993, pp. 27-31.
- Craig, J. J. 1988. *Adaptive Control of mechanical Manipulators*, Addison-Wesley Publishing Company, 1988.
- Czernik, D. E., Horve, L. A. 1993. *Handbook of Fluid Sealing*, McGraw-Hill, 1993.
- Dhanaraj, C. 1990. "Underwater Robotics", Report, C-CORE, Memorial University of Newfoundland, St.John's, NF, Canada, August 1990, 21 p.
- Dhanaraj, C. 1990. "Parallel Processing of Manipulator Dynamics Incorporating Frictional Effects", M.Eng. Thesis, Memorial University of Newfoundland. St.John's, NF, Canada, August 1990.
- Dimarogonas, A. 1989. *Computer Aided Machine Design*, Prentice Hall, 1989.
- Dupont, P. E. 1993. "The effect of friction in the forward dynamics problem", *The International Journal of Robotics Research*, Vol. 12, No. 2, April 1993, pp.164-179.
- Eckerle, W.A., Awad J.K. 1991. "Effects of free stream velocity on the three-dimensional flow region in front of cylinder", *Journal of Fluids Engineering*, transactions of the ASME, Vol.113, No. 1, March 1991, pp. 37-44.
- Farbrother, H.N.R., Stacey, B.A. 1993. "Aspects of Remotely Operated Vehicle Control-A Review", *Underwater Technology*, Volume 19, Number 1, Spring 1993, pp. 24-36.
- Fukuda, T., Hara, F. 1989. "Motion Control of Underwater Robotic Manipulator" (First Report, Adaptive Compensation Method of One Directional Fluid Force), Department of Engineering, Science University of Tokyo, Tokyo, Japan, 1989, pp. 2702-2706. (in Japanese)
- Gopalkrishnan, R., Grosenbaugh, M.A., Triantafyllou, M.S. 1992. "Influence of amplitude modulation on the fluid forces acting on a vibrating cylinder in cross-flow.", *International Journal of Offshore and Polar Engineering*, Vol. 2, No. 1, March 1992, pp.32-37.
- Guigne, J.Y. 1991. "A Supervised Neural Controller (SNC) for Underwater Robotic Applications, a Research Proposal", Report, C-CORE, Memorial University of Newfoundland, St. John's, NF, Canada, January 25, 1991, 23 p.

Horton, T.E., Golestanian, H., Feifarek, M.J. 1992 "Correlation of dynamic force coefficients based on wake volume scaling", Bluff-Body/Fluid and hydraulic Machine Interactions, ASME, Fluids Engineering Division FED Vol. 138, 1992, pp.63-76.

Kawamura, T., Takami, H., Kuwahara, K. 1986. "Computation of high Reynolds number flow around a circular cylinder with surface roughness.", Fluid Dynamics Research, Vol. 1, No. 2, December 1986, pp.145-162.

Kawato, M., Uno, Y., Isobe, M., Suzuki, R. 1988. "Hierarchical Neural Network Model for Voluntary Movement with Application to Robotics", IEEE Control System Magazine, April 1988, pp.8-15.

Kiya M., Tamura, H. 1989. "Flow about a circular cylinder in and near a turbulent plane mixing layer.", Journal of Fluid Engineering, Transactions of the ASME, Vol. 111, No. 2, June 1989, pp. 124-129.

Ko. N.W.M., Leung, Y.C., Chen, J.J.J. 1987. "Flow past V-groove circular cylinders.", AIAA Journal, Vol. 25, No. 6. June 1987, pp. 806-811.

Koterayama, W. 1991. "Recent advances in underwater technology in Japan.", Ocean Technologies and Opportunities in the Pacific for the 90's, Proceedings of Oceans 91, Vol. 2, IEEE, (IEEE cat. No. 91CH3063-5), pp. 868-875.

Lee, M. 1993. "Summary of MBARI/Stanford ARL Joint Underwater Robotics Research Program", Video Proceedings Eighth International Symposium on Unmanned Untethered Submersible Technology, University of New Hampshire, September 27-29, 1993.

Liceaga-Castro, E., Hong Q., Liceaga-Castro, J. 1991. "Modelling and Control of a Marine Robot Arm", IEEE Proceedings of the 30th Conference on Decision and Control, Brighton, England, 1991, pp. 704-705.

Mahesh, H., Yuh, J., Lakshmi, R. 1991. "Control of underwater robots in working mode.", IEEE International Conference on Robotics and Automation, Vol. 3, (IEEE cat. No. 91CH2969-4), pp. 2630-2635.

Makhortykh, G.V, Shcheglova, M.G. 1990. "Inertia and drag of cylinders oscillating in a fluid", Fluid Dynamics, Vol. 24, No. 4, January 1990, pp. 582-585.

Miyamoto, H., Kawato, M., Setoyama, T., Suzuki, R. 1988. "Feedback Error-Learning Neural Network for Trajectory Control of a Robotic Manipulator", Neural Networks, Vol. 1, 1988, pp. 251-265.

- Muggeridge, K.J., Hinchey, M.J. 1991. "Underwater Robot Control", Faculty of Engineering and Applied Science, Memorial University of Newfoundland, St. John's, NF, Canada, August 1991, 5 p.
- Nakamura, M., Hoshino, K., Koterayama, W. 1992. "Three-dimensional effects on hydrodynamic forces acting on an oscillating finite-length circular cylinder.", *International Journal of Offshore and Polar Engineering*, Vol. 2, No. 2, June 1992, pp. 81-86.
- Nam, S. 1990. "Higher-order boundary-layer solution for unsteady motion of a circular cylinder", *Journal of Fluid Mechanics*, Vol. 214, May 1990, pp.89-110.
- Niemann, H.J., Hoelscher, N., "Review of the recent experiments on the flow past circular cylinders.", *Journal of Wind Engineering and Industrial Aerodynamics*, Vol. 33, No.1-2, 1990, pp.197-209.
- Oldshue J. Y. 1983. *Fluid Mixing Technology*, McGraw-Hill Publications Co., 1983.
- Otsuka, K., Ikeda, Y. 1991. "Hydrodynamic forces acting on horizontal circular cylinder with an inclined angle to the wave crest in regular waves.", *International Journal of Offshore and Polar Engineering*, Vol. 1, No. 4, December 1991, pp. 278-283.
- Pap, R.M., Parten, C.R., Rich, M.L., Lothers, M., Thomas, C.R. 1991. "Underwater robotic operations using a decentralized adaptive neurocontroller.", *IEEE Conference on Neural networks for Ocean Engineering, Proceedings (IEEE cat. No. 91CH3064-3)*, pp. 197-206.
- Prandtl, L., Tietjens, O.J. 1934. *Applied Hydro and Aeromechanics*, Engineering Societies Monographs, 1934, 311 p.
- Rao, P., Kuwahara, K., Tsuboi, K. 1992. "Simulation of unsteady viscous flow around a longitudinally oscillating cylinder in a uniform flow.", *Applied Mathematics Modelling*, Vol. 6, No. 1, pp. 26-35.
- Radicioni, A., Magnelli, G., Raffaelli, E. 1992. "Snamprogetti's underwater robotics background. Experiences and new development.", *Offshore Technology Proceedings of the International Offshore Mechanics and Arctic Engineering Symposium*, Vol. 1, pt. B, ASME, pp.385-391.
- Reich, Jens-Georg; "C Curve Fitting for Scientists and Engineers", McGraw-Hill, 1992.
- Rivera, C., Hinchey, M.J. 1992. "Hydrodynamics of Simple Robot Arm/Body Configurations", *Ocean Engineering Research Centre*, July 1992.
- Sarpkaya, T., Isaacson, M. 1981. *Mechanics of Wave Forces on Offshore Structures*, Van Nostrand Reinhold Co., 1981, 651 p.

Sarpkaya, T. 1990. "On the effects of roughness on cylinders.", Proceedings of the Ninth International Conference on Offshore Mechanics and Arctic Engineering 1990, Vol. 1, pt. A, ASME, pp.47-55.

Sarpkaya, T. 1991. "Nonimpulsively started steady flow about a circular cylinder", AIAA Journal, Vol. 29, No. 8, August 1991, pp. 1283-1289.

Savill, A.M. 1989. "Effect on an adverse pressure gradient on the drag reduction performance of manipulators.", International Journal of Heat and Fluid Flow, Vol. 10, No. 2, June 1989, pp.118-124.

Schilling, Robert J. 1990. Fundamentals of Robotics: Analysis and Control, Prentice Hall, 1990.

Sharp J.J. 1981. Hydraulic Modelling, Butterworth & Co. Ltd, 1981

Sharp, J.J., Deb, A., Deb, M.K. 1992. Applications of matrix Manipulation in Dimensional Analysis Involving Large Number of Variables, Marine Structures 5 (1992) 333-348.

Sheglova, M.G., Makhortyk, G.V. 1988. "Inertial forces and resistance in a wave flow.", Hydrotechnical Construction, August 1988, pp. 96-103.

Sin, V.K. 1987. " Local force measurements on finite-span cylinders in a cross flow", Journal of Fluid Engineering, Transactions of the ASME, Vol. 109, No.2, June 1987, pp.136-143.

Slaouti, A., Stansby, P.K. 1992. "Flow around two circular cylinders by the random-vortex method.", Journal of Fluids and Structures, Vol. 6, No. 6, November 1992, pp. 641-670.

Sørensen, O. 1993. "Neural Networks Performing System Identification for Control Applications", International Conference of Artificial NN (Third: 1993, Brighton, England), pp. 172-176.

Sullivan, P.A, Hartmann, P.V., Graham, T.A. 1983. "Application Of System Identification Flight Analysis Techniques to the Pitch-Heave Dynamics of an Air Cushion Vehicle", Canadian Aeronautics and Space Journal, Vol 29, no. 4, December 1983, pp.348-370.

Sumer, B.M., Jensen, B.L., Fredsoe J. 1991. "Effect of a plane boundary on oscillatory flow around a circular cylinder", Journal of Fluid Mechanics, Vol. 225, April 1991, pp. 271-300.

Szirtes, T. 1992. "Scale-Model Tests Demand Clear Head and Sharp Mind", *Machine Design*, April 9, 1992, Vol. 64, No. 7

Tatsuno, M. 1989. "Steady flow around two cylinders at low Reynolds numbers.", *Fluid Dynamics Research*, Vol. 5, No. 1, June 1989, pp.49-60.

Velbitskii, F.V. , *Programming Technology*, Nauka, Kiev, 1984. (in Russian)

Wang, X. Dalton, C. 1991. "Numerical solutions for impulsively started and decelerated viscous flow past a circular cylinder", *International Journal of Numerical Methods for Fluids*, Vol. 12, No. 4, february 1991, pp.383-400.

West, G.S., Apelt, C.J. 1990. "Measurements of fluctuating effects on a circular cylinder in a uniform flow at subcritical Reynolds number", *Research Report Series-University of Queensland, Department of Civil Engineering*, No. CE110 July 1990, 27 p.

Westerman, A.W. 1991. "Neural network control of a robotic manipulator arm for undersea applications.", *Ocean Technologies and Opportunities in the Pacific for the 90's*, *Proceedings of Oceans 91*, Vol. 3, (IEEE cat. No.91CH3063-5), pp.1534-1538.

Yeung, R.W., Sphaier, S.H., Vaidhyathan, M. 1993. "Unsteady Flow About Bluff Cylinders.", *International Journal of Offshore and Polar Engineering*, Volume 3, No. 2, June 1993, pp. 81-92.

Yoerger, D.R., Cooke, J.G., Slotine, J.E. 1990. "The Influence of Thruster Dynamics on Underwater Vehicle and Their Incorporation Into Control System Design", *IEEE Journal of Oceanic Engineering*, Vol. 15, no. 3, July 1990, pp. 167-178.

Yoerger, D.R., Ulrich, N. 1991. "Dynamics and control of an underwater vehicle-manipulator system in constrained tasks." (Abstract), *Ocean Technologies and Opportunities in the Pacific for the 90's*, *Oceans 91*, Vol. 3, pp.1504.

Yoerger, D., Schempf, H., DiPietro, D. M. 1991. "Design and performance evaluation of an actively compliant underwater manipulator for full ocean depth.", *Journal of Robotic Systems*, Vol. 8, No. 3, June 1991, pp. 371-392.

Zdravkovich, M.M., Brand, V.P., Mathew, G., Weston, A. 1989. "Flow past short circular cylinders with two free ends.", *Journal of Fluid Mechanics*, Vol. 203, June 1989, pp.557-575.

Zomaya, A. Y., Nabhan T. M. 1993. "Centralized and decentralized neuro-adaptive robot controllers", *Neural Networks*, Vol. 6, 1993, pp. 223-244.

Zorpette, Glenn, "Autopilots of the Deep", *IEEE Spectrum*, August 1994, pp.38-44.

Appendix A

Neural Network System Identification

For the two-link configuration shown in figure 3-2, the net would look something like the one shown in figure 4-4. The net maps inputs, R_i , to outputs, R_o . The squashing of the middle layer outputs, R_m , is critical for a good map. Most NNI also squash the overall net output. The output from the net is:

$$R_o(J) = \sum_{J=1}^{MET} W_o(J,I) f(R_m(J)) \quad A-1$$

The output from the middle layer is:

$$R_m(J) = \sum_{I=1}^{KIN} W_i(J,I) R_i(I) \quad A-2$$

The weights between the input layer and the middle layer, W_i , form a matrix of NET by KIN, where NET is the number of neurons in the middle layer and KIN the number of inputs plus 1. The weights between the middle layer and the output layer, W_o , form a matrix of MET by KON, where MET is the number of neurons in the middle layer plus 1 and KON the number of outputs.

The goal is to find the output and input weights, W_o and W_i , which make the net output, R_o , match the target output R_t . One could find W_o and W_i by random search, but it would be very slow. Most NNI use back propagation to find the weights. The first step

is to form for each input an error:

$$e = (Ro - Rt) \quad \Lambda-3$$

The goal is to minimize the squared error from the net:

$$\sum^{KIN} \sum^{KON} e^2 \quad \Lambda-4$$

The sensitivities with respect to the weights are:

$$\frac{\partial \sum^{KIN} \sum^{KON} e^2}{\partial W} \quad \text{weights} \quad \Lambda-5$$

Here we use these in a Steepest Descent Iteration to find the weights. The method varies the parameters in a direction where the value of the fit criterion is decreasing most steeply. It has the advantage of being reliable as long as the adopted step length is short enough. The obvious disadvantage is that sometimes the step has to be so small that it can take endless cycles of iterations to find the desired fit. In the following expression the index "old" refers to the value obtained in the previous iteration, and "new" will be the result of the iteration being computed:

$$W_{(new)} = W_{(old)} - k \frac{\partial \sum \sum e^2}{\partial W_{(old)}} \quad \Lambda-6$$

The Steepest Descent Iteration has been used here to train the neural network identification routine, but it has been suggested in Reich 1992, that since it is slow but

reliable it could be used to find only an initial fit suitable as a starting point for a faster iteration method. The parameter k in 5-6 has been added to promote iteration stability.

The algorithms in this thesis have been represented using a flow chart type called R-Technology (Velbitskii, 1984). This method of representation was devised in the former Soviet Union, Ukraine, in the 1960's. It was supposed to evolve in to a programming language. It never did and was neither widely used even though it became a government standard in 1985 (GOST 19.005-85). Some of the advantages are the ability to write the full equation and the ease of representing multiple choices, something very inconvenient to represent using the traditional flow charts. Following is a very brief summary of how it works:

- 1) The arrows (figure A-1 a through f) function like a one way valve, the flow does not go against an arrow; e.g. from O the flow may go in the C, D or B directions but not in the A direction (figure A-1a).
- 2) Directions to the left have priority over directions to the right; e.g. if allowed, the flow will go first in the C or D directions before following direction B (figure A-1a).
- 3) The directions have a descending priority from top to bottom; e.g. the flow will try to follow direction A before following directions B or C (figure A-1b).
- 4) The condition above the line have to be complied with before the flow can follow the specified direction; e.g. If the condition is not satisfied the flow will not go from O to A and the statement below the line will not be executed (figure A-1c).

With the help of this system multiple choices, loops and iterations are readily and

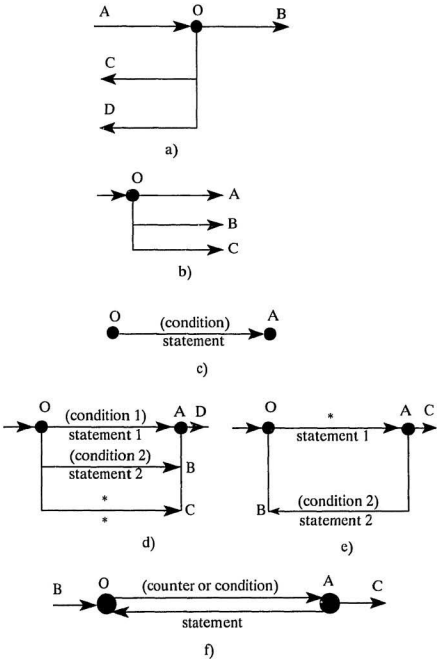


Figure A-1

clearly represented. An example of multiple choice is represented in figure A-1d, if condition 1 is satisfied the flow will go from O to A even if condition 2 is also satisfied. The * symbol means that there is no condition to be satisfied or no statement to execute, and that the flow may go from O to C unconditionally, however, this will only happen if neither condition 1 nor condition 2 are satisfied. Figure A-1e represents an example of an iteration. The * indicates that the flow will unconditionally go from O to A executing statement 1, then if condition 2 is satisfied it will go from A to B executing statement 2, which will be repeated until condition 2 is no longer satisfied, then the flow will follow the C direction. A combination of the two procedures described above are sufficient to represent basically any algorithm, however, sometimes is easier and more effective to use others, e.g. the counter or loop represented in figure A-1f. The statement will be executed until the counter reaches the end or until the condition is no longer satisfied, only then does the flow continue in the C direction.

Following are the flow charts of the Neural Network System Identification program.

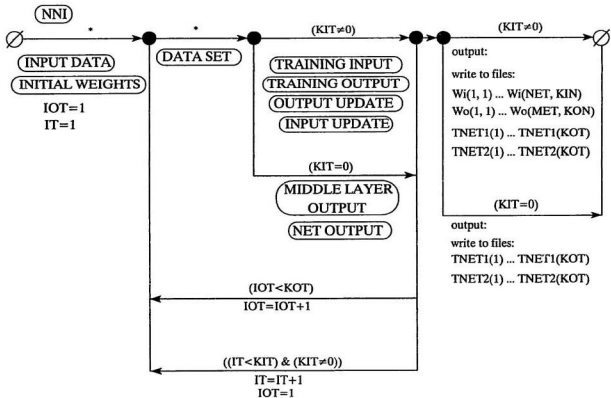


Figure A-2 Neural Network Identification Program

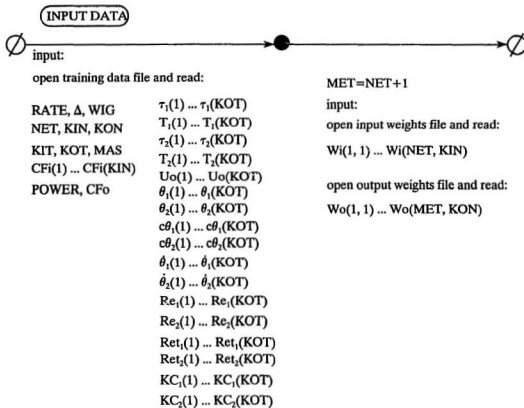
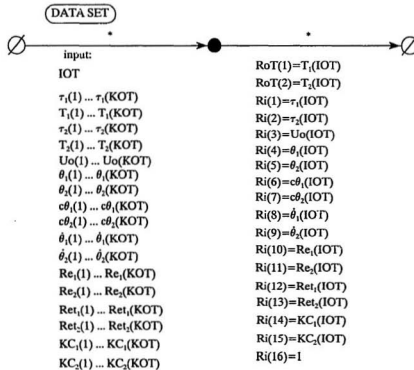
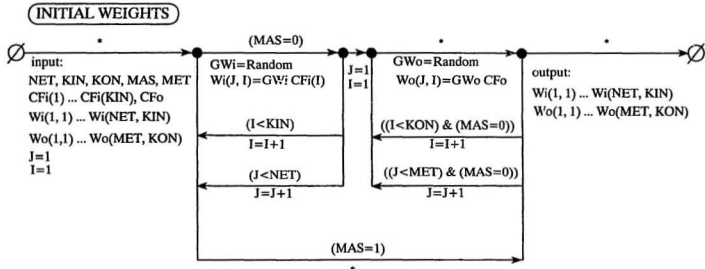


Figure A-3 Routine reading training data from a file



Note: In this case $KIN=16$ (The number of inputs), including a unity offset.

Figure A-4



Note: The parameter MAS indicates whether we want to use the weights from the file or start with random ones

Figure A-5 Initial Weights Calculation (Done randomly)

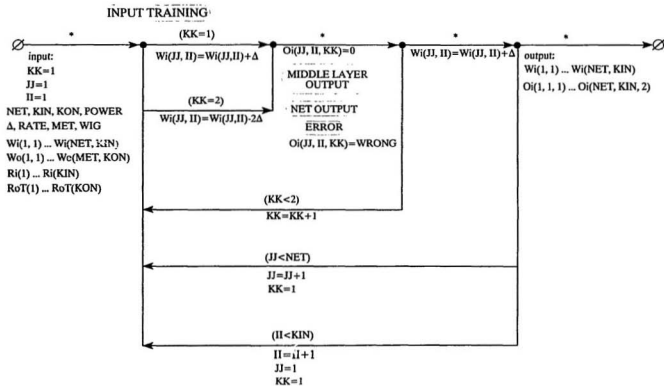


Figure A-6 Input Training Routine

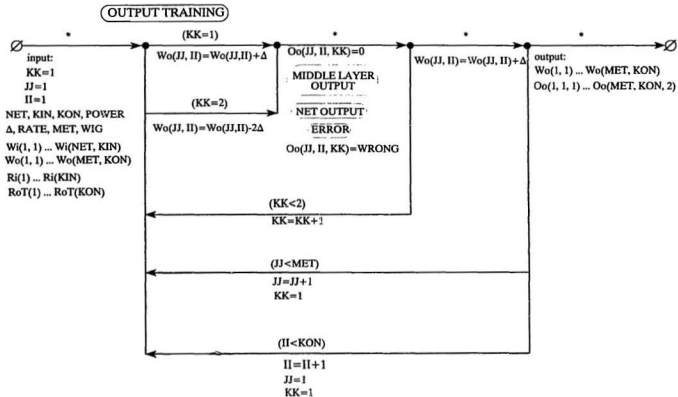


Figure A-7 Output Training Routine

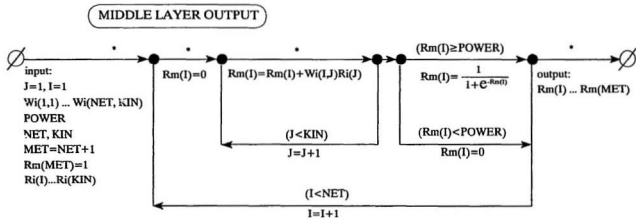


Figure A-8 Middle Layer Output Routine

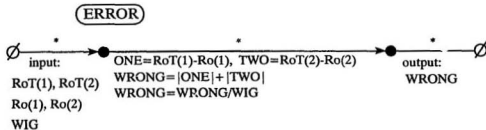
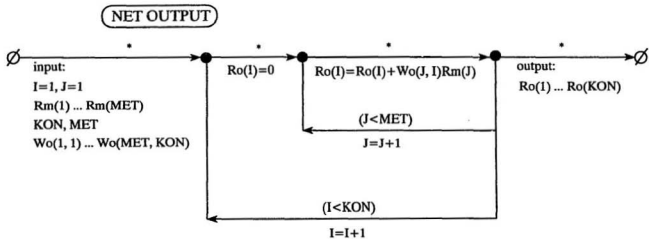


Figure A-9 Subroutines for the Net Output and the Error

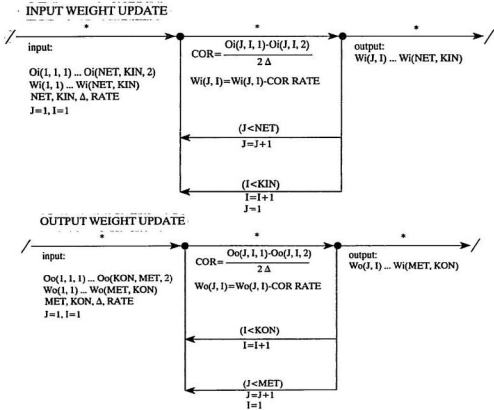


Figure A-10 Update of the Input Weights and the Output Weights

Appendix B

B.1 Neural Network Program Listing

```

C
C
C   NEURAL NETWORK IDENTIFICATION ROUTINE
C
C   Engineering and Applied Sciences
C
C   Memorial University of Newfoundland
C
C
C   The following program will compute the joint torques
C   of an underwater robot arm model after it is trained
C   with reliable experimental data
C
C   The input data:
C
C   TAU1,2           Computed Torques (Mathematical Model)      [N.m]
C   THETA1,2        Joint angles                                 [rad]
C   CTHETA1,2       Cosinuses of the Joint Torques
C   UO              Velocity of the Carrier                    [m/s]
C   THETADOT1,2    Angular Velocity at the Joints              [rad/s]
C   RE1,2          Reynolds Number
C   RET1,2         Rotational Reynolds Number
C   KC1,2          Modified Keulegan-Carpenter Number
C
C   The Target Data:
C
C   TORQUE1,2       Measured Joint Torques                      [N.m]
C
C   WI             Input Weights
C   WO             Output Weights
C   RI             Network Inputs
C   RO             Network Outputs
C   RM             Middle Layer Outputs
C   ROT           Target Outputs
C   NET           Number of Middle Layer Neurons
C   KIN           Number of Inputs
C   KON           Number of Outputs
C   KIT           Number of Training Iterations (If KIT = 0, Trained Network)
C   KOT           Number of Training Sets
C   TNET 1,2      Torque computed by the Neural Net

```

```

IMPLICIT REAL*8(A-H,O-Z)
REAL*8 L1,D1,L2,D2,NU,RHO
DIMENSION RI(17),RM(56),RO(2),ROT(2),WI(56,17),WO(56,2)
DIMENSION OI(56,17,2),OO(56,2,2),TORQUE1(200),TORQUE2(200)
DIMENSION TAU1(200),TAU2(200),TNET1(200),TNET2(200),UO(200),CFI(17)
DIMENSION THETA1(200),THETA2(200),CTHETA1(200),CTHETA2(200)
DIMENSION THETADOT1(200),THETADOT2(200)
DIMENSION KC1(200),KC2(200)RE1(200),RE2(200),RET1(200),RET2(200)

C
C  CONSTANT DATA
C
PI = 3.141592653589793D0
D1 = 4.D0*0.0254D0
D2 = 2.D0*0.0254D0
NU = 1.41E-06
RHO = 1000.D0

C
C  OPEN FILES
C
OPEN(5,file='nnid.d',status='old')
OPEN(6,file='nniwi.d',status='old')
OPEN(7,file='nniwo.d',status='old')
OPEN(8,file='nnit.o',status='old')

C
C  DATA
C
READ(5,*) RATE,DEL,WIG
READ(5,*) NET,KIN,KON
READ(5,*) KIT,KOT,MAS
READ(5,*) (CFI(I),I=1,14)
READ(5,*) POWER,CFO

C
C  INITIAL WEIGHTS
C
ISEED = 123457
MET = NET + 1
DO 1 J=1,NET
DO 1 I=1,KIN
IF(MAS.EQ.0) WI(J,I) = RAN(ISEED) * CFI(I)
IF(MAS.EQ.1) READ(6,*) WI(J,I)
1 CONTINUE
DO 2 J=1,MET
DO 2 I=1,KON
IF(MAS.EQ.0) WO(J,I) = RAN(ISEED) * CFO
IF(MAS.EQ.1) READ(7,*) WO(J,I)
2 CONTINUE

```

```

C
C   INPUT DATA
C
DO 3 IOT = 1, KOT
READ(5, *) ITAU1(IOT), TORQUE1(IOT), TAU1(IOT), TORQUE2(IOT)
READ(5, *) UO(IOT), THETA1(IOT), THETA2(IOT), CTHETA1(IOT)
READ(5, *) CTHETA2(IOT), THETADOT1(IOT), THETADOT2(IOT)
READ(5, *) RE1(IOT), RE2(IOT), RET1(IOT), RET2(IOT)
READ(5, *) KC1(IOT), KC2(IOT)
3 CONTINUE
IF(KIT.EQ.0) GO TO 18
DO 15 IT = 1, KIT
DO 15 IOT = 1, KOT

C
C   DATA ASSIGNMENT
C
ROT(1) = TORQUE1(IOT)
ROT(2) = TORQUE2(IOT)
RI(1) = 1.DO
RI(2) = THETADOT1(IOT)
RI(3) = THETADOT2(IOT)
RI(4) = UO(IOT)
RI(5) = CTHETA1(IOT)
RI(6) = CTHETA2(IOT)
RI(7) = RE1(IOT)
RI(8) = RE2(IOT)
RI(9) = RET1(IOT)
RI(10) = RET2(IOT)
RI(11) = KC1(IOT)
RI(12) = KC2(IOT)
RI(13) = THETA1(IOT)
RI(14) = THETA2(IOT)

C
C   TRAINING NETWORK
C   INPUT TRAINING
C
DO 8 II = 1, KIN
DO 8 JJ = 1, NET
DO 7 KK = 1, 2
IF(KK.EQ.1) WI(JJ,II) = WI(JJ,II) + DEL
IF(KK.EQ.2) WI(JJ,II) = WI(JJ,II) - 2.DO*DEL

C
C   MIDDLE LAYER OUTPUT
C
DO 5 I = 1, NET
RM(I) = 0.DO
DO 4 J = 1, KIN

```

```

RM(I) = RM(I) + WI(I,J) * RI(J)
4 CONTINUE
IF(RM(I).GE.POWER) RM(I) = 1.0DO/(1.0DO + DEXPI-RM(I))
IF(RM(I).LT.POWER) RM(I) = 0.DO
5 CONTINUE
RM(MET) = 1.0DO
C
C NET OUTPUT
C
DO 6 I = 1,KON
RO(I) = 0.DO
DO 6 J = 1,MET
RO(I) = RO(I) + WO(J,I) * RM(J)
6 CONTINUE
C
C ERROR
C
ONE = ROT(1)-RO(1)
TWO = ROT(2)-RO(2)
WRONG = DABS(ONE)/4.5DO + DABS(TWO)
WRONG = WRONG/WIG
OI(JJ,II,KK) = WRONG
7 CONTINUE
WI(JJ,II) = WI(JJ,II) + DEL
8 CONTINUE
C
C OUTPUT TRAINING
C
DO 13 JJ = 1,MET
DO 13 II = 1,KON
DO 12 KK = 1,2
IF(KK.EQ.1) WO(JJ,II) = WO(JJ,II) + DEL
IF(KK.EQ.2) WO(JJ,II) = WO(JJ,II) - 2.DO * DEL
C
C MIDDLE LAYER OUTPUT
C
DO 10 I = 1,NET
RM(I) = 0.DO
DO 9 J = 1,KIN
RM(I) = RM(I) + WI(I,J) * RI(J)
9 CONTINUE
IF(RM(I).GE.POWER) RM(I) = 1.0DO/(1.0DO + DEXPI-RM(I))
IF(RM(I).LT.POWER) RM(I) = 0.DO
10 CONTINUE
RM(MET) = 1.0DO

```

```

C
C   NET OUTPUT
C
  DO 11 I = 1,KON
  RO(I) = 0.DO
  DO 11 J = 1,MET
  RO(I) = RO(I) + WO(J,I) * RM(J)
11 CONTINUE
C
C   ERROR
C
  ONE = ROT(1) - RO(1)
  TWO = ROT(2) - RO(2)
  WRONG = DABS(ONE)/4.5DO + DABS(TWO)
  WRONG = WRONG/WIG
  OO(JJ,II,KK) = WRONG
12 CONTINUE
  WO(JJ,II) = WO(JJ,II) + DEL
13 CONTINUE
C
C   INPUT WEIGHT UPDATE
C
  DO 14 I = 1,KIN
  DO 14 J = 1,NET
  COR = (OI(J,I,1) - OI(J,I,2))/2.DO/DEL
  WI(J,I) = WI(J,I) - COR * RATE
14 CONTINUE
C
C   OUTPUT WEIGHT UPDATE
C
  DO 15 J = 1,MET
  DO 15 I = 1,KON
  COR = (OO(J,I,1) - OO(J,I,2))/2.DO/DEL
  WO(J,I) = WO(J,I) - COR * RATE
15 CONTINUE
C
C   PRINT INPUT WEIGHTS
C
  DO 16 J = 1,NET
  DO 16 I = 1,KIN
  WRITE(6,*) WI(J,I)
16 CONTINUE
C
C   PRINT OUTPUT WEIGHTS
C
  DO 17 J = 1,MET
  DO 17 I = 1,KON

```

```

WRITE(7,*) WO(J,I)
17 CONTINUE

18 CONTINUE
DO 23 IOT = 1,KOT
C
C DATA ASSIGNMENT
C
ROT(1) = TORQUE1(IOT)
ROT(2) = TORQUE2(IOT)
RI(1) = 1.DO
RI(2) = THETADOT1(IOT)
RI(3) = THETADOT2(IOT)
RI(4) = UO(IOT)
RI(5) = CTHETA1(IOT)
RI(6) = CTHETA2(IOT)
RI(7) = RE1(IOT)
RI(8) = RE2(IOT)
RI(9) = RET1(IOT)
RI(10) = RET2(IOT)
RI(11) = KC1(IOT)
RI(12) = KC2(IOT)
RI(13) = THETA1(IOT)
RI(14) = THETA2(IOT)
C
C TRAINED NETWORK
C MIDDLE LAYER OUTPUT
C
DO 20 I = 1,NET
RM(I) = 0.DO
DO 19 J = 1,KIN
RM(I) = RM(I) + WI(I,J)*RI(J)
19 CONTINUE
IF(RM(I).GE.POWER) RM(I) = 1.0DO/(1.0DO + DEXP(-RM(I)))
IF(RM(I).LT.POWER) RM(I) = 0.DO
20 CONTINUE
RM(MET) = 1.0DO

C
C NET OUTPUT
C
DO 21 I = 1,KON
RO(I) = 0.DO

```

```
DO 21 J = 1, MET
RO(I) = RO(I) + WO(J, I) * RM(J)
21 CONTINUE
TNET1(IOT) = RO(1)
TNET2(IOT) = RO(2)
22 CONTINUE
C
C PRINT NET OUTPUT
C
DO 23 IOT = 1, KOT
WRITE(8, *) TORQUE1(IOT), TNET1(IOT), TORQUE2(IOT), TNET2(IOT)
23 CONTINUE
C
C CLOSE FILES
C
CLOSE(5)
CLOSE(6)
CLOSE(7)
CLOSE(8)
STOP
END
```

B.2 Dynamic Equations of Motion Incorporating Hydrodynamic Forces

```

#include <math.h>
#include <stdio.h>
#include <iostream.h>
#include <fstream.h>
//
// application function : Morison's Equation Incorporated into the
//                               Equations of Motion
//
void calcul1( char*, char* );

void main()
{
    calcul1("myinput", "myoutput");
}

void calcul1 (char* input_file, char* output_file )

{

    // data

    float teta1, teta2;
    float dteta1, dteta2;
    float d2teta1, d2teta2;
    float u0, du0,d2u0, L1, L2;
    float D1, D2;
    float m1, m2;
    float M1,M2;
    float N1,N2,Lc1,Lc2;

    //
    // variables used during calculations
    //

    float faDy1,fbDy1, CaD1,CbD1;
    float faDy2,fbDy2, CaD2,CbD2;
    float faly1, faly2, fbly1, fbly2;
    float Cal1, Cal2, Cbl1, Cbl2;
    float Cdx;
    float fdx2, tauD12y, tauD11y, tauDy1, tauD12x, tauD1,tauD2;
    float tau1s, tau2s, tau1, tau2;

```

```
float A1, A2;
float B1, B2;
float Re1, Re2;
float Ret1, Ret2, KC1, KC2;
float uyL1, uyL2, ux1, ux2;
float taul1, taul2;
int signum1, signum2;

//constants

float nu = 1.41*pow10((-6));
float ro = 1000;

// load data from the file
ifstream infile (input_file);

infile >> L1;
infile >> L2;
infile >> D1;
infile >> D2;
infile >> u0;
infile >> du0;
infile >> d2u0;
infile >> teta1;
infile >> teta2;
infile >> dteta1;
infile >> dteta2;
infile >> d2teta1;
infile >> d2teta2;
infile >> m1;
infile >> m2;
infile >> Lc1;
infile >> Lc2;
infile >> ux1;
infile >> ux2;
infile >> Cdx;

//
teta1 = teta1*M_Pi/180;
teta2 = teta2*M_Pi/180;
A1 = dteta1;
A2 = dteta1 + dteta2;
B1 = u0*cos(teta1);
```

```

B2 = u0*cos(teta1 + teta2) + dteta1*L1*cos(teta2);
Re1 = B1*D1/nu;
Re2 = B2*D2/nu;
Ret1 = A1*L1*L1/nu;
Ret2 = A2*L1*L1/nu;

if (IA1 == 0)
    {KC1 = B1/L1/A1;}
else
    {KC1 = pow10(17);}

if (IA2 == 0)
    {KC2 = B2/L2/A2;}
else
    {KC2 = pow10(17);}

//
uyL1 = A1*L1 + B1;
uyL2 = A2*L2 + B2;
if (!uyL1 == 0)
    {signum1 = uyL1/abs(uyL1);}
else signum1 = 0;

if (!uyL2 == 0)
    {signum2 = (uyL2)/abs(uyL2);}
else signum2 = 0;

ux1 = u0*sin(teta1);
ux2 = u0*sin(teta1 + teta2) + dteta1*L1*sin(teta2);
if (A1 == 0)
    { faDy1 = 0.5*ro*D1*B1*abs(B1)*L1;
      fbDy1 = 0;
      CaD1 = L1/2;
      CbD1 = 0; }
else
    { if ((-B1/A1 <= 0) || (-B1/A1 >= L1))
      { faDy1 =
        0.5*ro*D1*signum1*((A1*L1 + B1)*pow10(3))/3/A1
        - B1*B1*B1/3/A1;
        fbDy1 = 0;
        CaD1 = L1/4*(3*A1*A1*L1*L1 + 6*B1*B1 + 8*B1*A1*L1)
        /(A1*A1*L1*L1 + 3*B1*B1 + 3*B1*A1*L1);
        CbD1 = 0;
      }
    }

```

```

else
{
    faDy1 = 0.5*ro*D1*signum1*(B1*B1*B1/3/A1);
    fbDy1 = 0.5*ro*D1*signum1*((A1*L1 + B1)/3/A1);
    CaD1 = -0.25 *B1/A1;
    CbD1 = 0.25*(3*A1*L1-B1)/A1;
};
};

if (A2 == 0) {
    faDy2 = 1/2*ro*D2*B2*abs(B2)*L2;
    fbDy2 = 0;
    CaD1 = L2/2;
    CbD2 = 0;
}

else
{
    if ((-B2/A2 <= 0) || (-B2/A2 >= L2))
    {
        faDy2 = 0.5*ro*D2*signum2 *(((A2*L2 + B2)*pow10(3))/3/A2
        - B2*B2*B2/3/A2);
        fbDy2 = 0;
        CaD2 = L2/4*(3*A2*A2*L2*L2 + 6*B2*B2 + 8*B2*A2*L2)/
        (A2*A2*L2*L2 + 3*B2*B2 + 3*B2*A2*L2);
        CbD2 = 0;
    }
    else
    {
        faDy2 = 0.5*ro*D2*signum2*(B2*B2*B2/3/A2);
        fbDy2 = 0.5*ro*D2*signum2*((A2*L2 + B2)/3/A2);
        CaD2 = -0.25 *B2/A2;
        CbD2 = 0.25*(3*A2*L2-B2)/A2;
    };
};

fdx1 = Cdx*M_Pi/8*ro*D1*D1*abs(ux1)*ux1;
fdx2 = Cdx*M_Pi/8*ro*D2*D2*abs(ux2)*ux2;
tauD12y = (CaD2 + L1*cos(teta2))*faDy2 + (CbD2 + L1*cos(teta2))*fbDy2;
tauD11y = CaD1*faDy1 + CbD1*fbDy1;
tauDy1 = tauD12y + tauD11y;
tauD12x = fdx2*L1*sin(teta2);
tauD1 = tauDy1 + tauD12x;
tauD2 = CaD2*faDy2 + CbD2*fbDy2;
N1 = du0*cos(teta1) - u0*dteta1*sin(teta1);
M1 = d2teta1;

```

```

N2      = d2teta1*L1*cos(teta2)- dteta1*L1*dteta2*sin(teta2)
          + du0*cos(teta1 + teta2)
          - u0*(dteta1*sin(teta1 + teta2) + dteta2*sin(teta2));
M2      = d2teta1 + d2teta2;
//

if ((-N1/M1 <= 0) || (-N1/M1 >= 0))
{
    faly1 = ro*M_PI*D1*D1/4*(N1*L1 + M1*L1*L1/2);
    fbly1 = 0;
    Cal1  = L1/3*((3*N1 + 2*M1*L1)/(2*N1 + M1*L1));
    Cbl1  = 0;
};

if ((-N1/M1 >= 0) || (-N1/M1 <= L1))
{
    faly1 = -ro*M_PI*0.25*D1*D1*N1*N1*M1/2;
    fbly1 = ro*M_PI*0.25*D1*D1*(M1*L1 + M1*L1*L1/2 + N1*N1/M1/2);
    Cal1  = -N1/M1/3;
    Cbl1  = (2*M1*L1-N1)/3/M1;
};

if ((-N2/M2 <= 0) || (-N2/M2 >= 0))
{
    faly2 = ro*M_PI*D2*D2/4*(N2*L2 + M2*L2*L2/2);
    fbly2 = 0;
    Cal2  = L2/3*((3*N2 + 2*M2*L2)/(2*N2 + M2*L2));
    Cbl2  = 0;
};

if ((-N2/M2 >= 0) || (-N2/M2 <= L2))
{
    faly2 = -ro*M_PI*0.25*D2*D2*N2*N2*M2/2;
    fbly2 = ro*M_PI*0.25*D2*D2*(N2*L2 + M2*L2*L2/2 + N2*N2/M2/2);
    Cal2  = -N2/M2/3;
    Cbl2  = (2*M2*L2-N2)/3/M2;
};

taul1 = faly1*Cal1 + fbly1*Cbl1;
taul2 = faly2*Cal2 + fbly2*Cbl2;

```

```

tau1s = (m1*Lc1*Lc1 + m1*m1*(3*D1*D1+D1*D1+4*L1*L1)/48
+ m2*(L1*L1+Lc2*Lc2+2*L1*Lc2*cos(teta2))
+ m2*(3*D2*D2+4*L2*L2)/48)*d2teta1
+ (m2*(L1*Lc2*cos(teta2)+Lc2*Lc2)
+ m2*(3*D2*D2+4*L2*L2)/48)*d2teta2
+ (m1*Lc1*cos(teta1)+m2*(L1*cos(teta1)
+ Lc2*cos(teta1+teta2)))*d2u0
- m2*L1*Lc2*sin(teta2)*(dteta1*dteta2+dteta2*dteta2/2);

```

```

tau2s = (m2*(L1*Lc2*cos(teta2)+Lc2*Lc2)
+ m2*(3*D2*D2+4*L2*L2)/48)*d2teta1
+ (m2*Lc2*Lc2+ m2*(3*D2*D2+4*L2*L2)/48)*d2teta2
+ (m2*Lc2*cos(teta1+teta2))*d2u0
+ (m2*L1*Lc2*sin(teta2))*d2teta2;

```

```
tau2 = tau2s;
```

```
tau1 = tau1s - tau2;
```

```
tau1 = tauD1 + tau1 + tau1;
```

```
tau2 = tauD2 + tau12 + tau2;
```

```

// write results to file
//
//
ofstream outfile(output_file);
outfile << tau1;
outfile << Torque1;
outfile << tau2;
outfile << Torque2;
outfile << teta1;
outfile << teta2;
outfile << dteta1;
outfile << dteta2;
outfile << u0;
outfile << KC1;
outfile << KC2;
outfile << Re1;
outfile << Re2;
outfile << Ret1;
outfile << Ret2;
outfile << cos(teta1);
outfile << cos(teta2);

```

```
}
```

Appendix C

Data set used to train the NNI (Neural Network Identification)

$\tau_{1,2}$	Torques at joints computed using the procedure in chapter 3	[N.m]
$T_{1,2}$	Target outputs (joint torques obtained from tests)	[N.m]
U_0	Velocity of the carrier	[m/s]
$\theta_{1,2}$	Joint angles (chapter 3)	[rad]
$C\theta_{1,2}$	Cosinuses of joint angles	
$\dot{\theta}_{1,2}$	Joint angular velocities	[rad/s]
$Re_{1,2}$	Reynolds number (chapter 3)	
$Ret_{1,2}$	Rotational Reynolds number (chapter 3)	
$KC_{1,2}$	Variation of the Keulegan-Carpenter number (chapter 3)	

τ_1	T_1	τ_2	T_2	U_0	θ_1	θ_2	$C\theta_1$	$C\theta_2$	$\dot{\theta}_1$	$\dot{\theta}_2$	Re_1	Re_2	Ret_1	Ret_2	KC_1	KC_2
3.055372	4.175	0	0	0.51	0	4.712389	1	0	0	0	36748.93	0	0	0	1.00E-17	1.00E+17
4.371027	4.65	0	0	0.61	0	4.712389	1	0	0	0	43954.61	0	0	0	1.00E-17	1.00E-17
5.921619	5.25	0	0	0.71	0	4.712389	1	0	0	0	51160.28	0	0	0	1.00E-17	1.00E-17
6.785017	7.25	0	0	0.78	0	4.712389	1	0	0	0	54763.12	0	0	0	1.00E-17	1.00E-17
7.20715	7.5	0	0	0.81	0	4.712389	1	0	0	0	58365.56	0	0	0	1.00E-17	1.00E-17
3.055372	2.5	0	0	0.51	0	4.712389	1	0	0	0	36748.93	0	0	0	1.00E-17	1.00E+17
8.688017	7.75	0	0	0.86	0	4.712389	1	0	0	0	61968.8	0	0	0	1.00E-17	1.00E+17
9.72762	9.25	0	0	0.91	0	4.712389	1	0	0	0	65571.83	0	0	0	1.00E-17	1.00E+17
10.82595	8.75	0	0	0.96	0	4.712389	1	0	0	0	69174.47	0	0	0	1.00E-17	1.00E+17
11.28171	9.75	0	0	0.98	0	4.712389	1	0	0	0	70615.5	0	0	0	1.00E-17	1.00E+17
11.98303	10.75	0	0	1.01	0	4.712389	1	0	0	0	72777.3	0	0	0	1.00E-17	1.00E+17
1.246698	1.75	0	0	0.4	0	628319	4.084071	0.809017	-0.58779	0	23218.05	0	0	0	1.00E-17	1.00E+17
1.947965	2.6225	0	0	0.5	0	628319	4.084071	0.809017	-0.58779	0	29147.56	0	0	0	1.00E-17	1.00E+17
2.899352	3.925	0	0	0.61	0	628319	4.084071	0.809017	-0.58779	0	35560.03	0	0	0	1.00E-17	1.00E+17
3.823927	5.225	0	0	0.71	0	628319	4.084071	0.809017	-0.58779	0	41389.54	0	0	0	1.00E-17	1.00E+17
5.11224	6.95	0	0	0.81	0	628319	4.084071	0.809017	-0.58779	0	47219.05	0	0	0	1.00E-17	1.00E+17
5.762861	7.45	0	0	0.86	0	628319	4.084071	0.809017	-0.58779	0	50133.81	0	0	0	1.00E-17	1.00E+17
6.45244	8.025001	0	0	0.91	0	628319	4.084071	0.809017	-0.58779	0	53048.56	0	0	0	1.00E-17	1.00E+17
7.180978	9	0	0	0.96	0	628319	4.084071	0.809017	-0.58779	0	55963.32	0	0	0	1.00E-17	1.00E+17

T_1	T_2	T_3	T_4	T_5	U_0	θ_1	θ_2	$C\theta_1$	θ_2	$\hat{\theta}_1$	$\hat{\theta}_2$	Re_1	Re_2	Ret_1	Ret_2	KC_1	KC_2	
13.826	14.95	-3.4658	-1.85	0.98	3.13263	3.22025	0.98683	0.98683	0	0	0	48092.7	34387.2	0	0	1.00E-17	1.00E-17	
-20.5148	-14.678	-5.6898	-1.8	0.88	3.19263	3.20025	0.98683	0.98683	0	0	0	-70518	-33207.8	0	0	1.00E-17	1.00E-17	
-21.9156	-15.525	-7.27418	-1.845	1.013	3.19263	3.20025	0.98683	0.98683	0	0	0	-72853.4	-34498.7	0	0	1.00E-17	1.00E-17	
-7.09594	-6.8	-0.53	-1.325	0.71	3.22859	3.20501	0.98619	0.95193	0	0	0	-5095.6	-16988.1	0	0	1.00E-17	1.00E-17	
-5.06224	-4.85	-0.3785	-1	0.5	3.22859	3.20501	0.98619	0.95193	0	0	0	-4309.5	-13804	0	0	1.00E-17	1.00E-17	
-3.51981	-3.425	-0.2028	-0.78	0.5	3.22859	3.20501	0.98619	0.95193	0	0	0	-3881.3	-11338.7	0	0	1.00E-17	1.00E-17	
-2.2056	-2.25	-0.125	-0.6	0.5	3.22859	3.20501	0.98619	0.95193	0	0	0	-3421.7	-9047.2	0	0	1.00E-17	1.00E-17	
-8.2666	-8.85	-6.8912	-1.66	0.811	3.22859	3.20501	0.98619	0.95193	0	0	0	-5821.7	-18383.1	0	0	1.00E-17	1.00E-17	
-10.4124	-10.25	-9.7778	-0.7	0.86	3.22859	3.20501	0.98619	0.95193	0	0	0	-61723	-19429.1	0	0	1.00E-17	1.00E-17	
-11.6284	-11.25	-10.7605	-2.175	0.91	3.22859	3.20501	0.98619	0.95193	0	0	0	-63522.1	-20623.8	0	0	1.00E-17	1.00E-17	
-12.9747	-12.425	-11.6885	-2.35	0.86	3.22859	3.20501	0.98619	0.95193	0	0	0	-68917.2	-21766.5	0	0	1.00E-17	1.00E-17	
-13.67	-13.475	-12.0215	-2.4523	0.88	3.22859	3.20501	0.98619	0.95193	0	0	0	-70777.6	-22256	0	0	1.00E-17	1.00E-17	
-14.183	-13.75	-12.0797	-2.65	1.012	3.22859	3.20501	0.98619	0.95193	0	0	0	-72643.9	-22846.5	0	0	1.00E-17	1.00E-17	
-14.818	-14.25	-12.1389	-2.85	0.86	3.22859	3.20501	0.98619	0.95193	0	0	0	-74510.2	-23437	0	0	1.00E-17	1.00E-17	
-4.4683	-4.725	-3.26489	-0.725	0.6	3.24631	3.209538	0.98452	0.91824	0	0	0	-4292.2	-13885.15	0	0	1.00E-17	1.00E-17	
-6.25697	-5.775	-4.552927	0.9	0.71	3.24631	3.209538	0.98452	0.91824	0	0	0	-60880	-16442.59	0	0	1.00E-17	1.00E-17	
-7.16914	-6.475	-6.032546	0.975	0.76	3.24631	3.209538	0.98452	0.91824	0	0	0	-54483.1	-17600.32	0	0	1.00E-17	1.00E-17	
-8.14348	-8.25	-7.19849	1.175	0.81	3.24631	3.209538	0.98452	0.91824	0	0	0	-58046.2	-18758.45	0	0	1.00E-17	1.00E-17	
-9.18814	-9.375	-8.36484	1.375	0.86	3.24631	3.209538	0.98452	0.91824	0	0	0	-61669.3	-19916.58	0	0	1.00E-17	1.00E-17	
-10.2002	-10.725	-9.532357	1.575	0.76	3.24631	3.209538	0.98452	0.91824	0	0	0	-65292	-21074.71	0	0	1.00E-17	1.00E-17	
-11.7811	-12.1975	-1.741751	0.575	0.81	3.24631	3.209538	0.98452	0.91824	0	0	0	-68915.2	-22232.84	0	0	1.00E-17	1.00E-17	
-13.0419	-13.625	-1.963419	0.6125	0.86	3.24631	3.209538	0.98452	0.91824	0	0	0	-72538.3	-23390.97	0	0	1.00E-17	1.00E-17	
-14.4802	-13.75	-2.446575	0.95	0.96	3.24631	3.209538	0.98452	0.91824	0	0	0	-76171.5	-24549.1	0	0	1.00E-17	1.00E-17	
-15.4862	-15.5	-2.580923	1.035	0.86	3.24631	3.209538	0.98452	0.91824	0	0	0	-79804.7	-25707.23	0	0	1.00E-17	1.00E-17	
-16.2814	-15.5	-2.713429	1.065	1.011	3.24631	3.209538	0.98452	0.91824	0	0	0	-83437.9	-26865.35	0	0	1.00E-17	1.00E-17	
-1.84472	-2.3	-0.197862	0.08	0.4	3.24631	3.216568	0.98452	0.60182	0	0	0	-2864.8	8233.519	0	0	1.00E-17	1.00E-17	
-0.30882	-3.45	-0.30889	0.16	0.5	3.24631	3.216568	0.98452	0.60182	0	0	0	-3881	12295.65	0	0	1.00E-17	1.00E-17	
-4.27981	-4.325	-0.63314	0.35	0.71	3.24631	3.216568	0.98452	0.60182	0	0	0	-4897.2	16307.2	0	0	1.00E-17	1.00E-17	
-7.3451	-7.375	-1.00001	0.525	0.81	3.24631	3.216568	0.98452	0.60182	0	0	0	-5914.4	20318.35	0	0	1.00E-17	1.00E-17	
-7.02042	-7.21	-0.711398	0.385	0.76	3.24631	3.216568	0.98452	0.60182	0	0	0	-64623.1	17445.42	0	0	1.00E-17	1.00E-17	
-7.87455	-8.475	-0.810127	0.455	0.81	3.24631	3.216568	0.98452	0.60182	0	0	0	-72450.3	26424.68	0	0	1.00E-17	1.00E-17	
-8.88445	-9.475	-0.91222	0.59	0.66	3.24631	3.216568	0.98452	0.60182	0	0	0	-80466.2	29182.98	0	0	1.00E-17	1.00E-17	
-10.0651	-10.15	-1.023506	0.6	0.81	3.24631	3.216568	0.98452	0.60182	0	0	0	-88485.4	31982.59	0	0	1.00E-17	1.00E-17	
-11.2016	-10.875	-1.137596	0.6625	0.86	3.24631	3.216568	0.98452	0.60182	0	0	0	-96504.6	34832.1	0	0	1.00E-17	1.00E-17	
-11.8732	-11.775	-1.15885	0.7625	0.88	3.24631	3.216568	0.98452	0.60182	0	0	0	-104523.2	37721.71	0	0	1.00E-17	1.00E-17	
-12.5448	-12.625	-1.18012	0.8625	0.91	3.24631	3.216568	0.98452	0.60182	0	0	0	-112542.4	40611.22	0	0	1.00E-17	1.00E-17	
-0.32344	0.25	-0.32467	0.775	0	3.26215	6.03838	0.99452	0.97026	0	0	0	-72322	24079.87	0	0	1.00E-17	1.00E-17	
-1.79559	-2.27	-0.86645	-1.475	0	0	0.977384	0	0.959193	0	0	0	0.95922	0.96819	0	0	1.62309	5	
-4.00726	-3.85	-1.40163	-1.86	0	1.370795	6.021386	-4.37E-08	0.959193	0	-1	0.76715	0	-281979	1.00E-17	0	0	1.00E-17	1.00E-17
-3.50071	-4.01	-1.32081	-1.86	0	1.570796	6.041052	-4.37E-08	0.959193	0	-2	2.2711	0	-33133	1.00E-17	0	0	1.00E-17	1.00E-17
-2.99376	-4.01	-1.24081	-1.86	0	1.770797	6.060718	-4.37E-08	0.959193	0	-2	3.8166	0	-32330	1.00E-17	0	0	1.00E-17	1.00E-17
-2.48681	-4.01	-1.16081	-1.86	0	1.970798	6.080384	-4.37E-08	0.959193	0	-2	5.3612	0	-31527	1.00E-17	0	0	1.00E-17	1.00E-17
-1.97986	-4.01	-1.08081	-1.86	0	2.170799	6.100050	-4.37E-08	0.959193	0	-2	6.9068	0	-30724	1.00E-17	0	0	1.00E-17	1.00E-17
-1.47291	-4.01	-1.00081	-1.86	0	2.370800	6.119716	-4.37E-08	0.959193	0	-2	8.4524	0	-29921	1.00E-17	0	0	1.00E-17	1.00E-17
-0.96596	-4.01	-0.92081	-1.86	0	2.570801	6.139382	-4.37E-08	0.959193	0	-2	10.0000	0	-29118	1.00E-17	0	0	1.00E-17	1.00E-17
-0.45901	-4.01	-0.84081	-1.86	0	2.770802	6.159048	-4.37E-08	0.959193	0	-2	11.5456	0	-28315	1.00E-17	0	0	1.00E-17	1.00E-17
0.04804	-4.01	-0.76081	-1.86	0	2.970803	6.178714	-4.37E-08	0.959193	0	-2	13.0912	0	-27512	1.00E-17	0	0	1.00E-17	1.00E-17
0.55709	-4.01	-0.68081	-1.86	0	3.170804	6.198380	-4.37E-08	0.959193	0	-2	14.6368	0	-26709	1.00E-17	0	0	1.00E-17	1.00E-17
1.06614	-4.01	-0.60081	-1.86	0	3.370805	6.218046	-4.37E-08	0.959193	0	-2	16.1824	0	-25906	1.00E-17	0	0	1.00E-17	1.00E-17
1.57519	-4.01	-0.52081	-1.86	0	3.570806	6.237712	-4.37E-08	0.959193	0	-2	17.7280	0	-25103	1.00E-17	0	0	1.00E-17	1.00E-17
2.08424	-4.01	-0.44081	-1.86	0	3.770807	6.257378	-4.37E-08	0.959193	0	-2	19.2736	0	-24300	1.00E-17	0	0	1.00E-17	1.00E-17
2.59329	-4.01	-0.36081	-1.86	0	3.970808	6.277044	-4.37E-08	0.959193	0	-2	20.8192	0	-23497	1.00E-17	0	0	1.00E-17	1.00E-17
3.10234	-4.01	-0.28081	-1.86	0	4.170809	6.296710	-4.37E-08	0.959193	0	-2	22.3648	0	-22694	1.00E-17	0	0	1.00E-17	1.00E-17
3.61139	-4.01	-0.20081	-1.86	0	4.370810	6.316376	-4.37E-08	0.959193	0	-2	23.9104	0	-21891	1.00E-17	0	0	1.00E-17	1.00E-17
4.12044	-4.01	-0.12081	-1.86	0	4.570811	6.336042	-4.37E-08	0.959193	0	-2	25.4560	0	-21088	1.00E-17	0	0	1.00E-17	1.00E-17
4.62949	-4.01	-0.04081	-1.86	0	4.770812	6.355708	-4.37E-08	0.959193	0	-2	27.0016	0	-20285	1.00E-17	0	0	1.00E-17	1.00E-17
5.13854	-4.01	0.03919	-1.86	0	4.970813	6.375374	-4.37E-08	0.959193	0	-2	28.5472	0	-19482	1.00E-17	0	0	1.00E-17	1.00E-17
5.64759	-4.01	0.11919	-1.86	0	5.170814	6.395040	-4.37E-08	0.959193	0	-2	30.0928	0	-18679	1.00E-17	0	0	1.00E-17	1.00E-17
6.15664	-4.01	0.19919	-1.86	0	5.370815	6.414706	-4.37E-08	0.959193	0	-2	31.6384	0	-17876	1.00E-17	0	0	1.00E-17	1.00E-17
6.66569	-4.01	0.27919	-1.86	0	5.570816	6.434372	-4.37E-08	0.959193	0	-2	33.1840	0	-17073	1.00E-17	0	0	1.00E-17	1.00E-17
7.17474	-4.01	0.35919	-1.86	0	5.770817	6.454038	-4.37E-08	0.959193	0	-2	34.7296	0	-16270	1.00E-17	0	0	1.00E-17	1.00E-17
7.68379	-4.01	0.43919	-1.86	0	5.970818	6.473704	-4.37E-08	0.959193	0	-2	36.2752	0	-15467	1.00E-17	0	0	1.00E-17	1.00E-17
8.19284	-4.01	0.51919	-1.86	0	6.170819	6.493370	-4.37E-08	0.959193	0	-2	37.8208	0	-14664	1.00E-17	0	0	1.00E-17	1.00E-17
8.70189	-4.01	0.59919	-1.86	0	6.370820	6.513036	-4.37E-08	0.959193	0	-2	39.3664	0	-13861					

T_1	T_2	T_3	U_0	θ_1	θ_2	$C\theta_1$	$C\theta_2$	$\hat{\theta}_1$	$\hat{\theta}_2$	Re_1	Re_2	Ret_1	Ret_2	KC_1	KC_2		
26.92468	0.5116	0.306581	0.135	0	4.376057	0	-0.42262	0	1.841678	65371.63	13858.9	0	283982.9	1.00E-17	0.43252		
26.97315	19.4625	5.292326	9.475	0	0.7613225	1	0.788011	0	2.028846	65371.63	24325.68	0	300780.3	1.00E-17	0.7120371		
23.02565	17.5225	4.801825	6.425	0.91	0.134464	0	0.424518	0	2.050762	65371.63	13855.88	0	304024.6	1.00E-17	0.410174		
11.43841	6.925	2.835868	3.155	0.91	0.1466077	1	0.424518	0	1.985312	65371.63	2427.05	0	284321.6	1.00E-17	0.1047395		
17.46639	0.3925	4.304822	4.1025	1.01	1.64061	0.991199	-0.986202	0.939199	3.977925	-5076.99	4434.65	0	530425.8	1.00E-17	7.52E-02		
17.46639	0.3925	4.304822	4.1025	1.01	1.64061	0.991199	-0.986202	0.939199	3.977925	-5076.99	4434.65	0	530425.8	1.00E-17	0.331465		
5.72480	11.965	1.868146	2.5175	0.6	1.64061	0.261779	-0.86E-02	0.153119	3.832941	-5076.99	3113.15	0	226401.2	1.00E-17	0.331465		
14.04586	10.0275	-3.264297	3.31	0.6	0.10472	0.68E-02	0.994522	0.99764	1.527163	42997.21	21398.61	0	226401.2	1.00E-17	0.846274		
14.57973	9.78	3.26127	4.055	0.6	0.10472	0.68E-02	0.994522	0.99764	1.527163	42997.21	21398.61	0	226401.2	1.00E-17	0.79662		
20.66073	13.3775	4.664832	4.805	0.71	0.10472	0.638842	0.994522	0.97026	1.985313	50860.02	25331.2	0	284321.7	1.00E-17	0.774587		
7.409519	6.83	3.01939	1.275	0.71	0.10472	4.729842	0.994522	1.78E-02	2.07257	50860.02	3117.433	0	307258.6	1.00E-17	0.32E-02		
16.85116	8.2025	4.051816	3.2025	0.71	0.10472	4.729842	0.994522	1.87788	2.07257	50860.02	12790.07	0	297856.1	1.00E-17	0.348654		
16.85116	8.2025	4.051816	3.2025	0.71	0.10472	4.729842	0.994522	1.87788	2.07257	50860.02	12790.07	0	297856.1	1.00E-17	0.348654		
20.91726	16.57	4.022789	4.95	0.81	0.10472	1.127173	0.994522	0.992548	1.41808	58946.22	26435.02	0	210222.8	1.00E-17	0.217312		
9.166511	3.1975	1.000853	3.1975	0.81	0.10472	1.291544	0.994522	0.775637	1.482529	58946.22	5067.569	0	219932.5	1.00E-17	0.207373		
8.720716	10.205	-0.3834	-0.41	0.81	0.10472	1.291544	0.994522	0.999339	1.527163	58946.22	-29111.9	0	226401.3	1.00E-17	0.15727		
14.68479	11.1675	2.872793	3.7825	0.81	0.10472	5.427974	0.994522	0.866059	1.439897	50946.22	21343.08	0	213464.1	1.00E-17	0.80986		
14.68479	11.1675	2.872793	3.7825	0.81	0.10472	5.427974	0.994522	0.866059	1.439897	50946.22	21343.08	0	213464.1	1.00E-17	0.80986		
14.68018	14.725	2.680191	1.57	0.61	0.972784	0.306001	0.559191	1.050014	-1.050014	24276.44	32317.28	305014.5	0	0.324237	1.00E-17	0.305145	
22.2501	17.8125	3.372204	2.8275	0.61	0.88176	0.401426	0.320505	0.920205	1.85088	40460.43	40812.32	263376.3	0	0.993003	1.00E-17	0.263765	
24.1801	21.085	3.542724	2.8275	0.61	0.243446	6.078839	0.970296	0.830848	0.830848	42848.97	41620.32	263376.3	0	1.13356	1.00E-17	0.263765	
26.4194	28.35	8.212886	4.5	1.01	1.291544	3.420848	0.278037	-0.96126	2.77071	20060.16	63370.1	-8570.0	0	0.3215	1.00E-17	0.100E-17	
30.0687	30.975	-7.8912	-3.21	1.01	5.133815	5.881796	0.350731	-0.20506	2.83616	28363.37	67116.7	-877255	0	0.2107	1.00E-17	0.100E-17	
30.0687	30.975	-7.8912	-3.21	1.01	5.133815	5.881796	0.350731	-0.20506	2.83616	28363.37	67116.7	-877255	0	0.2107	1.00E-17	0.100E-17	
-40.4522	-32.4725	3.144582	2.525	1.01	2.36194	2.36194	-0.70711	1.02111	-2.36194	2.36194	-1.146E-32	39.7162	-72304	0	0.463252	1.00E-17	0.100E-17
-23.5407	-22.5	3.746594	3.755	1.01	1.32645	3.359339	0.241922	-0.9703	-2.59818	2.59818	17606.42	59361.3	-603025	0	-0.14251	1.00E-17	0.100E-17
1.925855	6.4725	-7.48249	-1.405	0.71	1.954769	2.321288	-0.74681	-0.682	0.981748	-0.981748	-19165	-25741.3	303665.3	0	-0.14251	1.00E-17	0.100E-17
0.994077	2.1525	0.385002	0.245	0.71	3.984818	4.471239	-0.79801	0.893007	1.134465	-1.13447	-40314.3	13239.83	380902	0	-0.74678	1.00E-17	0.100E-17
4.26884	8.4	-1.73708	-1.2525	0.71	1.605303	2.030354	-4.45E-02	-0.89101	0.872684	-0.872684	-785.47	25311.6	289824.8	0	-4.20E-02	1.00E-17	0.100E-17
21.5825	20.7	3.66505	3.665	0.91	0.525311	4.72202	0.650509	0.88E-02	1.24342	0.348066	-42011.86	25347.87	384642.5	236104.2	0.226067	0.178774	
18.50714	15.3825	4.31642	3.78	0.91	1.342004	4.928282	0.224951	1.330814	0.361799	14750.41	39008.72	411635	236104.2	0.226067	0.178774		
4.741252	3.1125	3.062924	1.8825	0.91	1.565334	4.991642	0.83867	0.279638	1.636863	-4.36E-02	-54993	20459.68	51285.6	239338.4	-0.68609	0.765929	
30.5767	-28.6375	-4.263242	3.8225	0.91	6.230825	5.270895	0.89963	0.129919	0.610865	65481.77	-7398.13	286917.3	232870	1.433002	1.082077		

UNABLE TO FILM MATERIAL ACCOMPANYING THIS THESIS (I.E.
DISKETTE(S), SLIDES, MICROFICHE, ETC...).

PLEASE CONTACT THE UNIVERSITY LIBRARY.

INCAPABLE DE MICROFILMER LE MATERIEL QUI ACCOMPAGNE CETTE THESE
(EX. DISQUETTES, DIAPOSITIVES, MICROFICHE (S), ETC...).

VEUILLEZ CONTACTER LA BIBLIOTHEQUE DE L'UNIVERSITE.

NATIONAL LIBRARY OF CANADA
CANADIAN THESES SERVICE

BIBLIOTHEQUE NATIONALE DU CANADA
LE SERVICE DES THESES CANADIENNES



